In presenting the dissertation as a partial fulfillment of the requirements for an advanced degree from the Georgia Institute of Technology, I agree that the Library of the Institute shall make it available for inspection and circulation in accordance with its regulations governing materials of this type. I agree that permission to copy from, or to publish from, this dissertation may be granted by the professor under whose direction it was written, or, in his absence, by the Dean of the Graduate Division when such copying or publication is solely for scholarly purposes and does not involve potential financial gain. It is understood that any copying from, or publication of, this dissertation which involves potential financial gain will not be allowed without written permission.

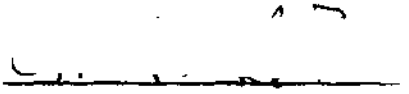

3/17/65
b

SEDIMENT TRANSPORT FUNCTIONS WITH SPECIAL EMPHASIS ON LOCALIZED SCOUR

A THESIS

Presented to

The Faculty of the Graduate Division

by

Albert Richard LeFeuvre

In Partial Fulfillment

of the Requirements for the Degree

Doctor of Philosophy

in the School of Civil Engineering

Georgia Institute of Technology

May, 1965

SEDIMENT TRANSPORT FUNCTIONS WITH SPECIAL

EMPHASIS ON LOCALIZED SCOUR

Approved:

Date Approved by Chairman: 5/27/65

ACKNOWLEDGMENTS

The writer wishes to thank all those who assisted in the preparation of this thesis. Dr. M. R. Carstens, thesis advisor and chairman of the reading committee, deserves special thanks for suggesting the study and for his encouragement and patient guidance. The other members of the reading committee were Professor C. E. Kindsvater and Dr. C. S. Martin. Mr. Homer Bates, laboratory technician, provided invaluable assistance in the construction of the experimental apparatus.

The writer wishes to acknowledge with sincere appreciation the financial assistance provided by the Ford Foundation Fellowship in Aid of Engineering Teaching.

TABLE OF CONTENTS

TABLE OF CONTENTS (Continued)

LIST OF TABLES

LIST OF TABLES (Continued)

LIST OF ILLUSTRATIONS

NOMENCLATURE

Symbol	Quantity
b	width of sediment bed
C_D	coefficient of drag
C_L	coefficient of lift
d	mean diameter of sediment particle
F_D	drag force
F_L	lift force
F_S	surface force
$\mathbb{F}_{sd}$	sediment Froude number
$\mathbb{F}_{sdc}$	critical sediment Froude number
k_1, k_2	undetermined coefficients
g	acceleration due to gravity
m	slope
M_o	moment about O
n_1, n_2	moment arm about O
q_s	sediment discharge per unit width
Q_s	sediment discharge
Q_{si}	sediment discharge into scour hole
Q_{so}	sediment discharge out of scour hole
$\mathbb{R}_d$	local Reynolds number
$\mathbb{R}_*$	shear Reynolds number
s	specific gravity
t	time

NOMENCLATURE (Continued)

Symbol	Quantity
u	local velocity a distance y from boundary
u_*	shear velocity
U_∞	velocity outside the boundary layer
V_d	local velocity a distance d from boundary
V_k	local velocity a distance k from boundary
$V_{\delta'}$	local velocity at the edge of the laminar sublayer
$\bar{V}$	average velocity in the main flow
$\forall$	volume of scour hole
W	submerged weight of the particle
X	distance from beginning of boundary layer growth to cross-section of interest
X_e	length of flat plate boundary layer growth equivalent to actual test section
X_c	distance from beginning of boundary-layer growth to start of transition to turbulent boundary layer
y	distance from boundary at which the local velocity is u
γ	specific weight of fluid
γ_s	specific weight of sediment
δ'	thickness of laminar sublayer
δ^*	displacement thickness of boundary layer
τ_o	boundary shear stress
τ_c	critical boundary shear stress
ρ	mass density of fluid
μ	absolute viscosity of fluid
ν	kinematic viscosity of fluid

SUMMARY

The subject of this study is an investigation into the mechanisms of localized scour. The object is to determine a sediment-transport function relating transport to the flow parameter of local velocity and the sediment parameters of specific weight and diameter.

Scour is the excavation and removal of bed material by fluid in motion. A general mathematical expression can be formulated from the principle of conservation of mass which encompasses all scouring situations

$$Q_{so} - Q_{si} = \frac{d\forall}{dt} \qquad (1)$$

In equation (1), Q_{so} is the rate that sediment is being removed from the scour hole, Q_{si} is the rate that sediment is being transported into the scour hole, $\forall$ is volume of the scour hole, and $d\forall/dt$ is the rate of change of $\forall$. A uniform stream such as a canal section is stable when the LHS of equation (1) is zero. A canal is scouring when the capacity of the stream to excavate and remove sediment is greater than the rate of sediment inflow. In such a case $Q_{so} > Q_{si}$ for which $d\forall/dt > 0$. The increase in volume $\forall$ of a reach is accomplished by a degradation of the bed and/or an increase in the canal width.

Localized scour occurs in the vicinity of obstructions placed in the flow. The increase in velocity adjacent to an obstruction is accompanied by an increased capacity to carry sediment as compared with unobstructed areas of the bed. In many situations a scour hole adjacent

to the obstruction will occur as a result of this localized increase of capacity to excavate and remove bed material.

Localized scouring situations are characterized by the continual change of boundary geometry with time; that is, local scour is a case of unsteady flow. The total volume of material carried away by the flow in a given period of time may be determined from the change in boundary geometry.

The mechanisms of local scour are investigated by transforming this normally unsteady-state situation to the steady state by supplying sediment to the scour area from an external source at the same rate at which it is being transported away from the scour area by the flow. The scouring fluid is water flowing in a three-inch diameter plexiglass tube. This flow is adjusted to produce an equilibrium between the rate of scour and the rate of sediment supply. Sediment is supplied to the scour area from a metal tube. The sediment is forced from the tube by a piston driven by a positive drive mechanism. Two different scour situations are investigated. One is transport from a plane bed of sediment which forms a boundary at the main flow. The second is transport from the bottom of an idealized scour hole.

The relationship between the rate of sediment transport away from a scour area and the independent variables of flow, fluid and sediment properties is investigated. Sediment-transport rates are varied more than one hundred fold. Six different sediments are tested. Mean diameters range from 0.106 mm to 0.585 mm. Specific gravity of the sediment material varies from 1.20 for Lucite, to 8.75 for nickel.

Incipient-motion analysis attempts to define the magnitude of the

surface force on the bed particles at which movement of these particles commences. The incipient-motion condition is determined for each sediment for both the plane-bed and scour-hole situations.

In the plane-bed tests, the particles are submerged in a well-behaved laminar boundary layer. Thus, it is possible to determine a local velocity in the neighborhood of the bed particles. The local velocity a distance of one grain diameter from the boundary is selected as the significant velocity for flow-induced surface forces on the bed particles.

The most significant conclusion of this study is that the boundary-shear force is not a measure of the surface forces on individual particles which are submerged in a laminar boundary layer. For the flat bed immersed in a laminar boundary layer, the measured transport rate, Q_s, will not correlate with the boundary shear stress, τ_o. Correlation of the data can be achieved only by using the velocity in the vicinity of the particles. Surface forces upon the bed particles are proportional to the drag force given by the conventional drag relationship, as shown by

$$\text{Drag force} \propto C_D d^2 \frac{\rho V_d^2}{2}$$

in which C_D is a coefficient of drag, d is the particle diameter, ρ is the mass density of the fluid, and V_d is a reference velocity in the vicinity of the particle. The rate of sediment transport is proportional to the surface force upon the bed particles. Hence a transport function for bed particles submerged in a laminar boundary layer must involve the drag on the particles due to the local velocity V_d rather than the boundary-shear stress τ_o.

Incipient motion is the limiting condition of zero transport for the sediment-transport function. It follows from above, therefore, that the criteria for incipient motion of particles submerged in a laminar boundary layer should involve the drag on the particles due to the local velocity V_d, rather than the boundary shear stress τ_o.

Using the local velocity in the vicinity of the particles and the conventional relationship between drag coefficient and Reynolds number, the form of the Shields diagram can be predicted for that portion of the Shields diagram in which the bed particles are submerged in a laminar layer.

A non-dimensionalized sediment-transport function requires a reference discharge. The fluid flow involved in the transport mechanism is only that flow near the sediment-water interface. Such a flow can be formed from the local velocity V_d and the flow area within one grain diameter of the bed. Hence the sediment-transport function is

$$\frac{Q_s}{V_d db} \propto C_D \frac{V_d^2}{(s-1)gd}$$

in which Q_s is the rate of sediment transport, b is the width of the bed, C_D is the coefficient of drag, s is the specific gravity of the sediment material, and g is the acceleration due to gravity.

At high values of the local Reynolds number, $V_d d/\nu$, the coefficient of drag on bed particles becomes independent of the local Reynolds number.

For transport from the bottom of a scour hole the sediment-transport function is approximated by the power relationship

$$\frac{Q_s}{V_d db} \propto \left[\frac{V_d}{\sqrt{(s-1)gd}}\right]^7$$

CHAPTER I

INTRODUCTION

Definition of the Problem

The subject of this study is an investigation into the mechanisms of localized scour. The object is to determine a sediment-transport function relating transport to the flow parameter of local velocity and the sediment parameters of specific weight and diameter.

Scour is the excavation and removal of bed material by fluid in motion. A general mathematical expression can be formulated from the principle of conservation of mass which encompasses all scouring situations

$$Q_{so} - Q_{si} = \frac{d\forall}{dt} \qquad (1)$$

In equation (1), Q_{so} is the rate that sediment is being removed from the scour hole, Q_{si} is the rate that sediment is being transported into the scour hole, $\forall$ is volume of the scour hole, and $d\forall/dt$ is the rate of change of $\forall$. A uniform stream such as a canal section is stable when the LHS of equation (1) is zero. A canal is scouring when the capacity of the stream to excavate and remove sediment is greater than the rate of sediment inflow. In such a case $Q_{so} > Q_{si}$ for which $d\forall/dt > 0$. The increase in volume $\forall$ of a reach is accomplished by a degradation of the bed and/or an increase in the canal width.

Localized scour occurs in the vicinity of obstructions placed in

the flow. The increase in velocity adjacent to an obstruction is accompanied by an increased capacity to carry sediment as compared with unobstructed areas of the bed. In many situations a scour hole adjacent to the obstruction will occur as a result of this localized increase of capacity to excavate and remove bed material.

Localized scouring situations are characterized by the continual change of boundary geometry with time. That is, local scour is a case of unsteady flow. The total volume of material carried away by the flow in a given period of time may be determined from the change in boundary geometry.

A great simplification in the study of local scour would be achieved if a steady state situation could be attained. The only way to transform localized scour to steady-state conditions is to supply sediment to the scour hole from an external source, at a rate equal to the rate of scour. Steady state occurs naturally when the approaching flow carries sediment with it.

If the approaching flow contains no sediment then Q_{si} must be zero. This is an important practical case as for instance the flow spilled from a reservoir. Any sediment carried down from the watershed will have been deposited behind the dam so that water passed over the spillway will be clear of sediment. Indeed this modification of the character of the water flowing downstream from a dam causes gradual erosion of the downstream river channel. If this important case of scour by a flow of clear water is to be transferred to steady state conditions, sediment must be supplied to the scour area from some other external source than from the oncoming flow.

In this investigation sediment was supplied to the scour area by feeding sediment directly into the bottom of the scour hole. In this way the scour-hole dimensions were held constant.

The object was to determine the relationship between the flow, fluid properties, and sediment properties, and the rate of sediment transport away from the scour area. From eq. (1) we see that if $\frac{d\Psi}{dt} = 0$

$$Q_{so} = Q_{si}$$

That is to say, if the boundary geometry is held constant it is possible to measure the rate of sediment transport away from the scour area Q_{so} by measuring the rate of sediment supply Q_{si}.

Idealized Flow Boundaries

A free surface flow over an erodible bed yields a flow geometry which is very difficult to control. For this reason this study departed from any attempt to model a naturally occurring scour situation and constructed an idealized scour area. The main flow was confined within a closed conduit to avoid variations of flow area with changes in depth. The scour-area geometry was fixed by the solid boundaries of an idealized scour hole and by maintaining the water-sediment interface at a fixed elevation.

Rate of Sediment Transport

With the boundary geometry fixed so that $\frac{d\Psi}{dt} = 0$ it was possible to obtain a measure of the rate of sediment transport as accurately as the rate of sediment supply could be measured. The rate of sediment supply was measured by means of a positive-displacement supply mechanism as described in Chapter II. With the rate of sediment transport

accurately measurable, the object was to determine the effect, on this transport rate, of variations in flow velocity and sediment properties.

History and Review of Literature

The relationships controlling the transport of particulate solids by a flowing fluid have been sought by engineers for many years. These relationships are applicable to many engineering problems such as erosion and deposition in stream channels, solids transport in pipe lines, and local scour around structures. Engineers must predict the effect on a stream channel, of changes due to planned improvements such as dams or dredging. This problem has been approached in many different ways over the years. Rule-of-thumb methods were replaced by empirical relationships based on a combination of field and laboratory data. Unfortunately, this approach yielded a large number of different equations, each one of which was of limited application. Brown (1) lists several of the better-known formulas of this type.

In recent years a considerable effort has been made to discover the fundamental relationships between flow, fluid, and sediment properties. For the most part these data have been reported in terms of dimensionless parameters which make it easier to compare the results of different investigators.

The total sediment transport in a stream is often arbitrarily subdivided into "suspended load" and "bed load" transport. Suspended load includes all material carried in the main flow and held above the bed by fluid turbulence. The application of the theory of fluid turbulence to this mechanism has assisted greatly in explaining and predicting suspended-load transport. Actually there is a continuous exchange of

particles from the bed to the main flow by entrainment and turbulent diffusion which is just balanced by the rate at which other particles fall back to the bed. Existing knowledge concerning transfer of sediment between the bed and the main flow is very meager. On the other hand, considerable experimental knowledge has been accumulated about the sediment particles which move by rolling and sliding over the bed -- bed-load transport.

Bed-load transport includes the movement of sediment particles by sliding, rolling, or jumping short distances in the direction of flow. The particles never rise more than a few grain diameters above the bed. This mode of transport is affected greatly by the boundary layer. The drag force acting on the bed particle, and tending to transport it, is a function of the fluid velocity and flow pattern in the neighborhood of the particle. Practically all of the existing bed-load formulas follow the classical DuBoy's (2) assumption that the rate of transport is proportional to the magnitude of the average shear force exerted on the bed.

Many of the formulas for bed-load transport include the concept of a threshold condition known as incipient motion. Incipient-motion analysis attempts to define the magnitude of the surface force on the bed particles at which movement of these particles commences. The classical study of Shields (3) demonstrated a correlation between this critical surface force and the sediment properties of diameter and specific weight. The Shields parameter

$$\frac{\tau_c}{(\gamma_s - \gamma)d} \qquad (2)$$

in which τ_c is the boundary shear stress at incipient motion, γ_s is the specific weight of the sediment, γ is the specific weight of the fluid, and d is the diameter of the sediment particle, was shown to be constant for the case where the bed particles projected into the turbulent flow above the laminar sublayer. For the case where the bed particles were immersed in the laminar sublayer the Shields parameter became a function of d/δ' where δ' was the thickness of the laminar sublayer.

In spite of the superficial differences in the common bed-load transport functions, Garde (4) has shown that all are two parameter functions. The sediment-transport parameter q_s/u_*d is a function of the parameter $u_*^2/(s-1)gd$, in which q_s is the rate of sediment transport per unit width, u_* is the shear velocity as given by $u_* = \sqrt{\tau_o/\rho}$, s is the specific gravity of the sediment, and g is the gravitational acceleration. In all likelihood such a complex phenomenon cannot be adequately represented by relation of only two dimensionless variables. In fact, Brooks (5) presents convincing experimental evidence that u_* is unsuitable as an independent variable by virtue of the large variation of boundary resistance resulting from the change from a duned bed to a flat bed.

Another area of interest in the field of sediment transport is the problem of localized scour. Areas of high velocity around bridge piers and other structures cause intense local scour which is often so serious as to endanger the foundations of the structure. Naturally occurring scour is an unsteady flow phenomenon because the flow pattern must change as the scouring action changes the boundary geometry. Rouse (6) performed a series of experiments with an idealized scour situation.

He observed the change of scour-hole geometry as a function of time using a vertical two-dimensional jet directed down upon an erodible bed. Laursen (7) conducted a similar set of experiments with a horizontal rather than a vertical jet.

In the experiments of Rouse and Laursen, as in natural scour situations, the process is self limiting because of the progressive change in boundary geometry. The scouring action continues at a decreasing rate until the local velocities in the eroding area are reduced to the level at which the resulting surface forces are unable to overcome the resisting forces of gravity. Laursen showed that such a limit existed.

Several other investigators have studied local scour in models of such engineering problems as flow around bridge piers and spur dikes. Laursen and Toch (8) studied scour around a model bridge pier. M. Ahmed (9) studied the scour patterns around spur dikes in a model of the Sutlej River. In all of these investigations the scour-hole geometry changed with time until the local scouring velocities were reduced to the level at which the shear equaled the critical shear for incipient motion. Thus $\frac{d\Psi}{dt}$ was zero only when Q_{so} became zero.

To the best of the writer's knowledge, the experiments reported herein are the only ones in which the scour mechanism was studied as a steady-state condition. The fixed boundary geometry made it possible to measure the rate of sediment transport directly. In earlier investigations the rate of sediment transport could be obtained only by differentiating the boundary-geometry function. This was done by

Carstens (10) in a reanalysis of the studies reported by Rouse (6) and Laursen (7).

CHAPTER II

EXPERIMENTAL APPARATUS

The object of the study was to provide a scour area such that sediment could be supplied to the area at the same rate as it was transported away by the flow. This required the following elements:

(1) A flow of fluid to produce the scour and transport the sediment away from the scour area.

(2) An external supply of sediment to the scour area to establish an equilibrium condition.

(3) A scour area of controlled geometry which could be acted upon by the flow of fluid and supplied with sediment from an external source.

The Scouring Flow

The scouring flow of fluid was produced with water flowing in a three-inch diameter plexiglass tube. This closed-conduit flow avoided the variation of flow cross section with variations in depth associated with free-surface flows. Water was supplied to this test section from a six-inch diameter pipe through an elliptical contraction section. The six-inch diameter pipe was connected to the constant-head tank of the recirculating water supply of the hydraulics laboratory of the School of Civil Engineering. The flow leaving the test section was carried in a three-inch diameter pipe to a weir tank where the discharge was measured and the transported sediment was trapped for reuse. The flow over the weir

returned to the sump of the recirculating system. Figure 1 is a schematic diagram of the apparatus and Figure 2 is a photograph of the equipment.

The flow of water through the apparatus was measured by means of a 90-degree triangular weir. This weir was calibrated gravimetrically.

The head on the weir was measured to the nearest thousandth of a foot by means of a hook gage mounted in the weir tank. This degree of accuracy was checked by changing the hook elevation one thousandth of a foot up or down and observing the change in the relationship of the hook point to the water surface. In all but the higher flows reported there was a clearly discernible change in the relationship between the hook point and the water surface with a change in hook elevation of 0.001 ft. At high flow rates the water surface was disturbed such that the head on the weir could be estimated to only the nearest five hundredths of a foot. At the highest velocities in the test section of about 12 ft/sec, the error in hook-gage reading corresponded to an error of 0.1 ft/sec which is a relative error of 0.83 per cent. At the lowest velocities of about 0.5 ft/sec, the error in hook-gage reading corresponded to an error of about 0.01 ft/sec which is a relative error of 2.0 per cent. Over the major portion of the range of velocities the relative error was less than one per cent.

The Supply of Sediment

Supply Mechanism

Sediment was forced upward to the scour area through a vertical copper tube by means of a piston. The piston displacement was produced by the following series of positive mechanical drives:

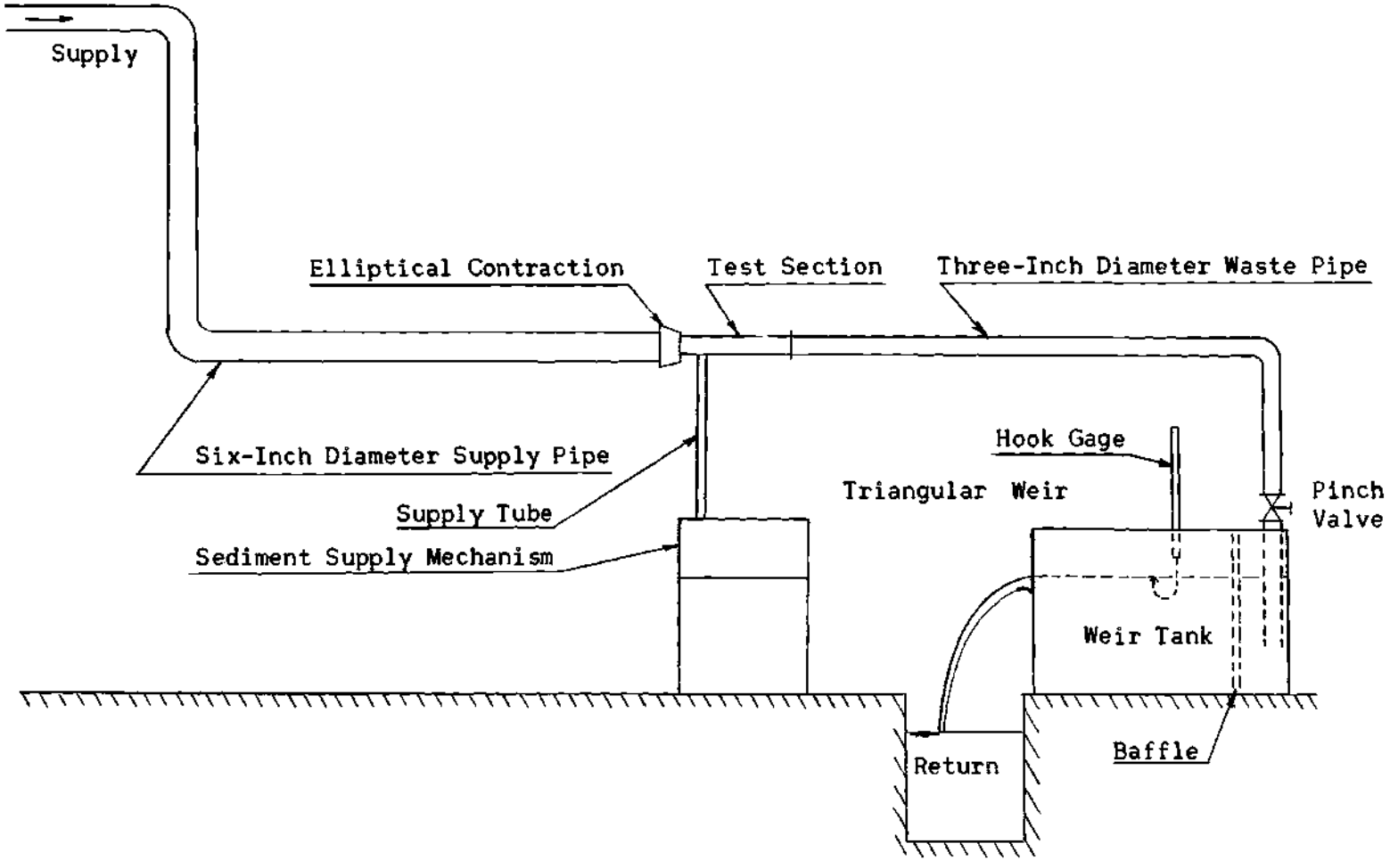

Figure 1. Schematic of Experimental Apparatus.

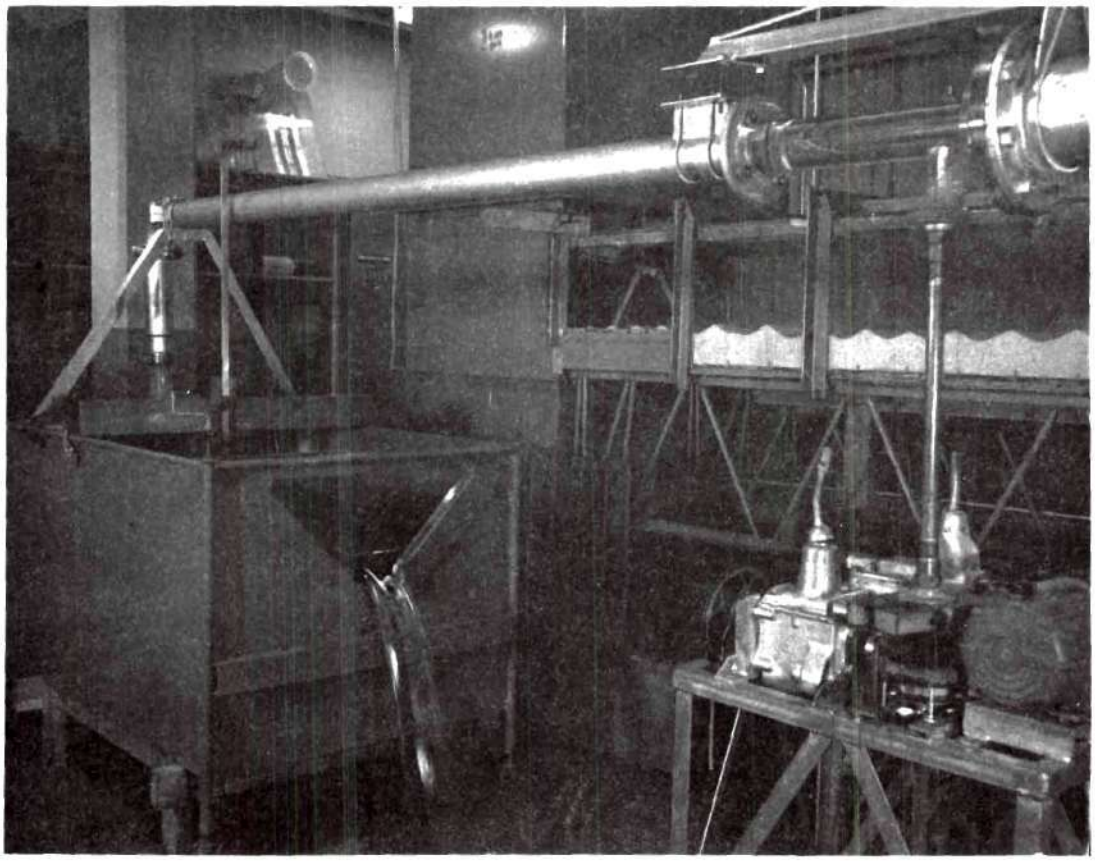

Figure 2. Photograph of General Arrangement of Apparatus.

Element	Speed Ratio
1800 RPM Synchronous Motor	
Worm-Wormwheel Speed Reducer	30:1
Packard Automotive Transmission	1:1 to 3.176:1 in 4 steps
Chain and sprocket drive	4:13 or 13:4
Ford Automotive Transmission	1:1 to 3.745:1 in 4 steps
Crown and pinion bevel-gear set	6:1
Screw thread and drive nut	1/8 inch per revolution

The final vertical motion of the piston was achieved by the rotation of the drive nut which was threaded on the piston shaft. Since the positive-drive mechanism was driven by a synchronous motor, the piston speed was determined exactly for a given setting of the transmissions and chain and sprocket ratio. The transmission ratios were determined by counting the number of teeth on the various gears. The piston speeds for the various arrangements of transmission levers are given in Table 1.

As shown in Table 1, the total range of piston speed was from 0.0257 inches/min. to 3.250 inches/min. or a variation of 126.5:1.

The piston assembly consisted of a flexible cup, such as is used in the hydraulic brake system of automobiles, supported by a nylon disc which was just slightly smaller than the inside diameter of the pipe. The nylon disc transmitted any side thrust, from the screw drive, to the pipe walls and allowed the flexible cup to be squeezed against the pipe walls by the water pressure thus assuring a water-tight fit.

The rate of sediment supply was determined from the known rate of piston displacement and the measured porosity of the sediment. The rate of piston displacement was known to a high order of accuracy because of the nature of the drive mechanism. Thus, the uncertainty in the sediment supply rate was due to the variability of the porosity of the sediment in the supply tube. As described in Appendix B, the porosity of each sediment was measured experimentally under conditions similar to those encountered during a run. The porosity was about 50% with a maximum measured deviation from average of about 3% or a relative error of 6%. This maximum error occurred with only the two largest grain sizes. All other sediments showed less than 4% relative error in porosity measurements.

Sediment

Six different sediments were tested in this study. The physical properties of these sediments were measured as described in Appendix B, and are listed in Table 2.

The Scour Area

The scour area geometry was controlled by the fixed plexiglass boundaries. The sediment-water interface was the only movable portion of the bounding geometry. At the equilibrium condition this interface was held at a reference level which was common to all runs. In one phase of the investigation this interface was located at the bottom of an idealized scour hole. In another phase of the investigation the interface was located at the boundary of the main flow.

The scour hole was formed in a two-inch diameter plexiglass tube which intersected the three-inch diameter main tube at right angles. The main flow was horizontal. The two-inch diameter tube extended

vertically downward. The geometry of the scour hole was controlled further by inserting a 60 degree wedge as shown in Figure 3.

The second phase of the problem required a bed of sediment in the main test section which could be fed from beneath in a manner similar to the idealized scour hole. This was accomplished by replacing the 2" dia. scour hole with a 1" dia. opening directly over the supply tube as shown in Figure 4. The resulting scour area was a small patch of sediment bed over the tube opening. The main flow acted directly on this bed and carried sediment downstream.

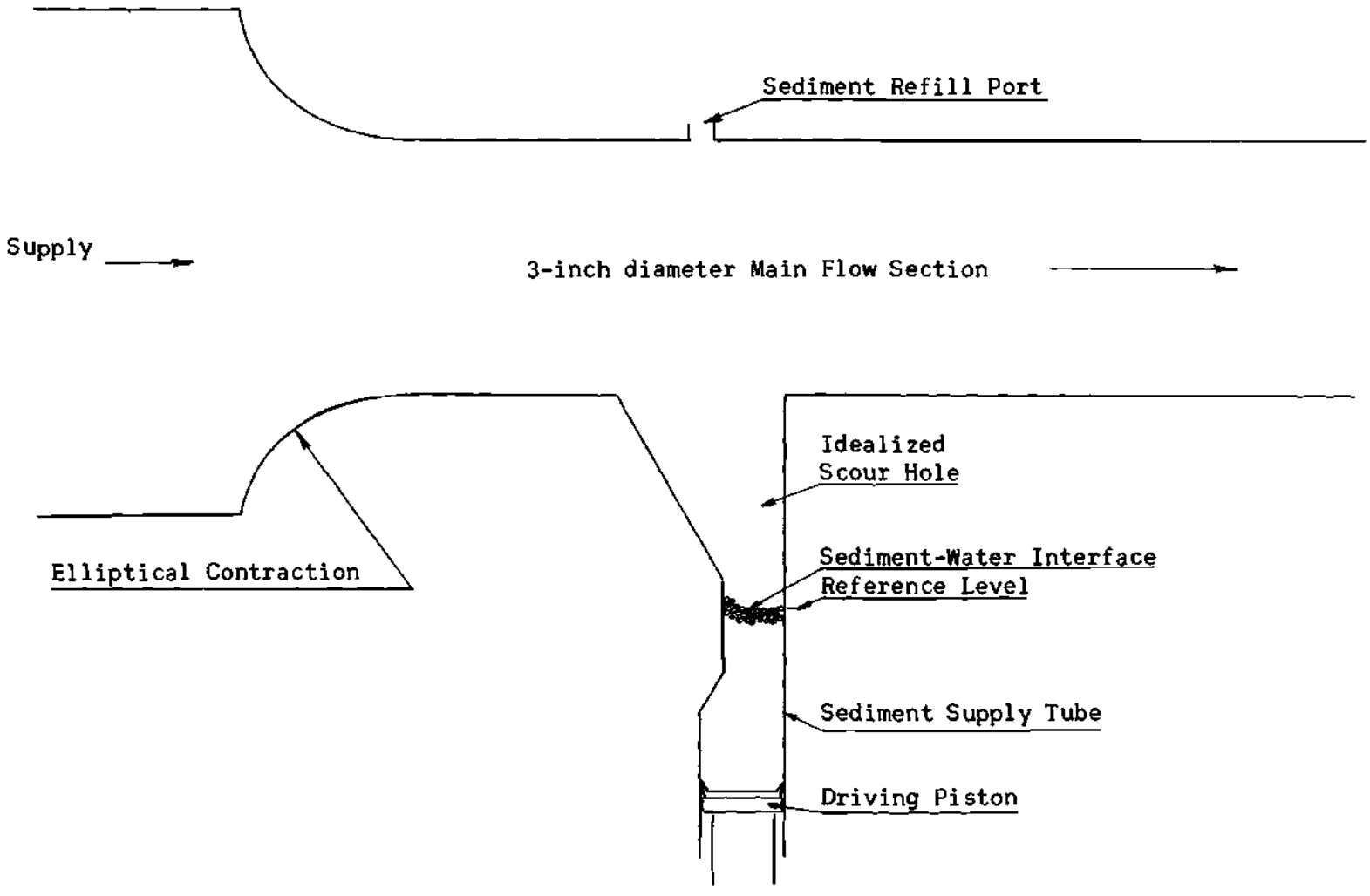

Figure 3. Definitive Sketch of Test Section for Scour-Hole Tests.

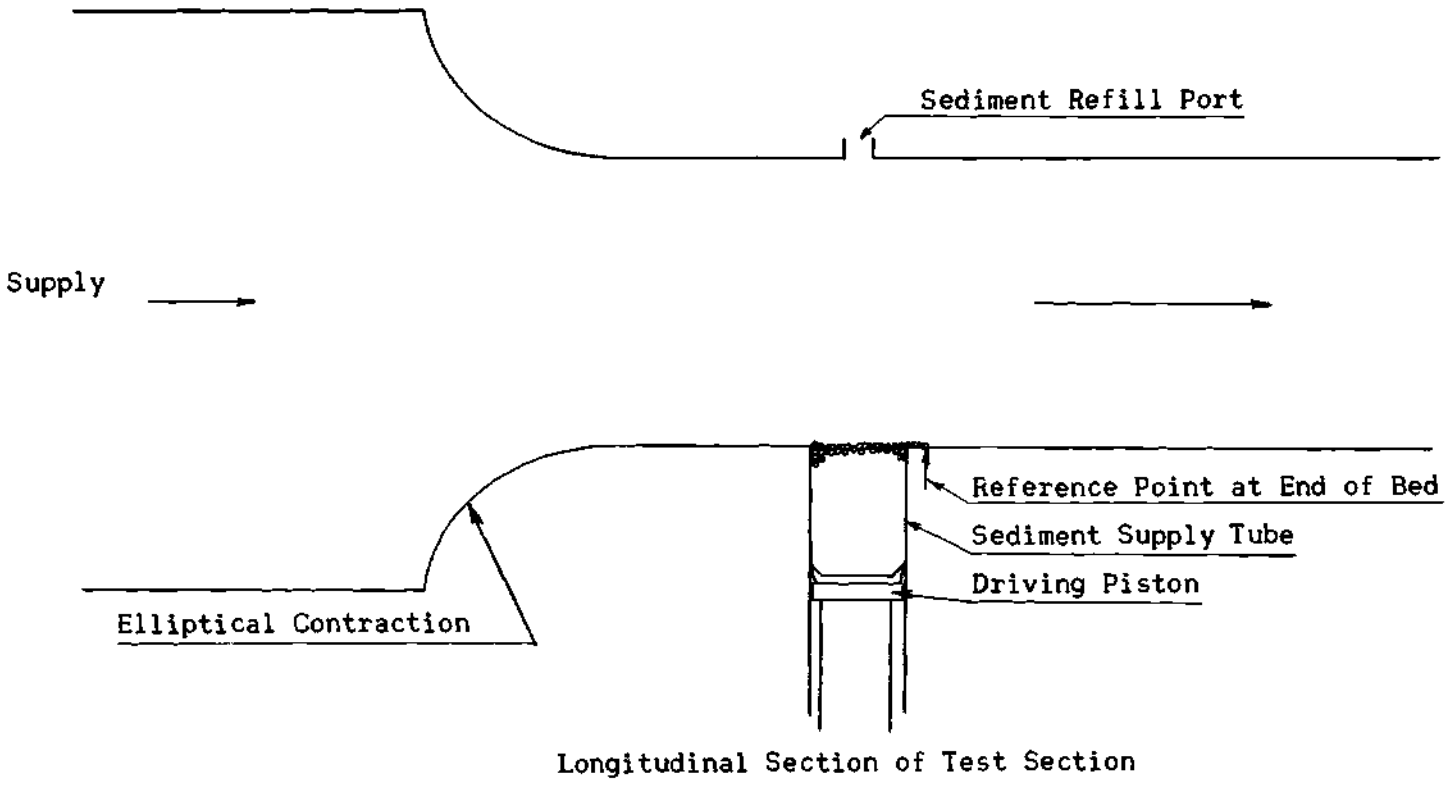

Figure 4. Definitive Sketch of Test Section for Plane-Bed Tests.

CHAPTER III

EXPERIMENTAL PROCEDURE

The experimental program consisted of two separate studies. In one, scour from the bottom of an idealized scour hole was investigated. In the other, sediment transport from a plane bed of sediment on the boundary of the main flow section was investigated. Auxiliary tests were determinations of the velocity profile in the test section (Appendix A). The method of determining the sediment properties; mean diameter, specific gravity, and porosity are presented in Appendix B.

Sediment Transport Rate

The operating procedure was devised to establish the equilibrium condition in which the rate of sediment transport was equal to the rate of sediment supply. In this condition the sediment-water interface was stationary. At the same time it was necessary to keep the interface located at the reference level so that the flow geometry would be the same from run to run. With equilibrium established at the reference level the rate of flow was measured. All of this had to be accomplished in the limited time required to empty the sediment supply tube. A run started with the refilling of the sediment supply tube. The sediment was poured through a small opening in the top of the test section and fell directly into the scour hole and thence to the supply tube. During this filling process the supply tube was tapped lightly to provide a uniform packing of the sediment. When the required amount of sediment

had been placed in the supply tube, the filling port was closed and the test section was filled with water by opening the valve in the supply pipe. The automotive transmissions were set to give the desired sediment feed rate and the feed mechanism was started. When the water-sediment interface approached the reference level the pinch valve in the outlet pipe was opened to establish a flow of water in the test section. If the interface was above the reference level the main flow was increased and vice versa. The pinch valve was adjusted until the interface held steady at the reference level. In this condition the scour hole geometry was the same as for all other runs and the rate of sediment supply was equal to the rate of sediment transport. The head on the triangular weir was measured by means of a hook gage and the water temperature was measured with a thermometer suspended in the weir tank.

Plane Bed Tests

For sediment transport from a plane bed the sediment in the end of the supply tube formed a small sediment bed at the wall of the main test section. By trial it was found that as the level of the sediment mound at the mouth of the supply tube rose, an extension of the sediment bed developed downstream from the supply tube. This single layer of sediment particles was able to stay on the smooth plexiglass tube because it was sheltered from the main flow by the mound upstream from it. The length of this extension bed was, therefore, a sensitive indicator of the height of the mound at the mouth of the supply tube. For a given supply rate, the flow velocity was adjusted until the downstream end of this bed extension coincided with a reference position which was half an

inch downstream from the supply tube opening. The sediment bed was observed best from above. This was facilitated by installing a mirror above the test section. Data of the 84 runs are tabulated in Tables 9 - 14, inclusive.

Scour Hole Tests

For sediment transport from the bottom of an idealized scour hole the sediment-water interface was maintained at a constant level three-tenths of an inch below the bottom of the sixty-degree slope (Figure 3). Experience indicated that this level was stable for all rates of sediment supply. Data of the 148 runs are tabulated in Tables 3-8, inclusive.

Incipient Motion

For both the plane-bed and scour-hole tests, an attempt was made to determine the flow velocity which just started transport of grains away from the scour area. This condition is often termed incipient motion. In these tests the interface or bed configuration was established at standard reference conditions and the flow was then reduced to well below the incipient-motion value. The flow was gradually increased and at each step increase the condition of the bed was described. Usually the first few step increases caused no change in the bed. As the flow was increased, occasional rocking of isolated particles could be observed. At still higher flows one or two isolated particles would be carried away by the water. Next the whole bed would appear agitated and finally groups of particles would be swept away at frequent intervals. Fortunately the range of velocities from no transport to obvious transport was relatively small. The incipient motion data are tabulated in Table 30.

CHAPTER IV

ANALYSIS OF EXPERIMENTAL DATA

The principal objective of the following analysis is to explain rationally the sediment transport rate as a function of the independent variables. In order to achieve this objective the sediment-transport rate is assumed to be a function of the external forces on a typical particle. Initially the limiting condition, that is, zero rate of sediment transport will be analyzed. The limit of zero transport occurs at incipient motion when the forces on the particles are just sufficient to lift and to roll some particles over their neighbors.

Incipient Motion (Plane Bed)

At the condition of incipient motion, the particle rolls out of the recess in the bed. Referring to Figure 5, the particle-to-particle reaction R_2 will be zero at incipient motion. Writing a moment equation about the remaining point of contact at O,

$$\Sigma M_o = 0 = F_S n_1 - W n_2 \tag{3}$$

in which F_S is the surface force on the particle, and W is the submerged weight. Solving for the force ratio

$$F_S/W = n_2/n_1 \tag{4}$$

The lever-arm ratio n_2/n_1 can be expected to be constant if the flow pattern remains similar. Similar flow patterns imply (a) similar approach

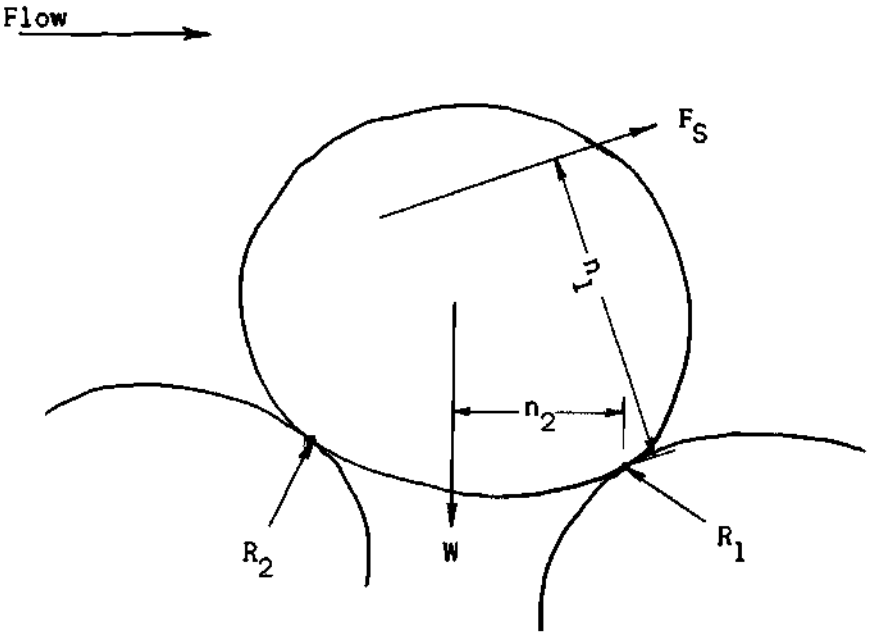

Figure 5. Forces on a Typical Sediment Particle.

velocity distribution and (b) the absence of drastic changes such as a large shift in the separation pattern.

The weight force W is the submerged weight. Assuming a spherical particle

$$W = (\gamma_s - \gamma) \frac{d^3\pi}{6} \tag{5}$$

in which γ_s is the specific weight of the sediment, γ is the fluid specific weight, and d is the particle diameter.

The surface force F_S is conventionally separated into orthogonal components of drag, F_D and lift, F_L.

$$F_S = \sqrt{(F_D)^2 + (F_L)^2} \tag{6}$$

In addition both the lift and drag force are conventionally expressed as

$$F_L = C_L \frac{d^2\pi}{4} \frac{\rho V^2}{2} \tag{7}$$

and

$$F_D = C_D \frac{d^2\pi}{4} \frac{\rho V^2}{2} \tag{8}$$

in which ρ is the fluid density, V is a reference velocity, and C_L and C_D are coefficients which are experimentally determined.

Substituting the expressions for the forces, equations (5), (6), (7), and (8), into equation (4),

$$\frac{n_2}{n_1} = \frac{4}{3} \sqrt{(C_L)^2 + (C_D)^2} \; \frac{V^2}{(s-1)gd} \qquad (9)$$

in which s is γ_s/γ.

A logical choice of the reference velocity to be used in equation (9) is the velocity within the laminar boundary layer at a height d from the wall. By means of a supplementary experimental study (Appendix A), the boundary layer which developed in the flow through the contraction has been shown to be laminar at the section where the fluid meets the layer of particles. By virtue of the way in which the flow was adjusted, the layer of particles was about one diameter in thickness. In other words, the patch of particles protruded to a height d from the pipe wall. Hence the velocity, V_d, at this elevation appears to be a sensible choice as a reference velocity.

The order of magnitude of the lever-arm ratio n_2/n_1 can be established. When a plane bed of particulate material is inclined, some surface particles begin to roll when the angle of inclination is sufficiently large. This angle is called the angle of repose. Using an angle of repose of 45 degrees, the value of n_2 would be $d/2\sqrt{2}$. The line of action of the surface forces would certainly intersect the particle, that is, $n_1 < d$. Furthermore by considering that the surface forces are on the upper surface of the particle, the lever arm n_1 would be greater than $d/2$. Thus

$$\frac{1}{2\sqrt{2}} < \frac{n_2}{n_1} < \frac{1}{\sqrt{2}} \tag{10}$$

and

$$\frac{n_2}{n_1} = k_1 = k_1(R_d) \tag{11}$$

in which R_d is the local Reynolds number $V_d d/\nu$.

The order of magnitude of the coefficients of lift and drag are difficult to estimate inasmuch as no other experiments have been made in which a layer of particles was immersed in a laminar boundary layer. Nearly similar flow situations which have been studied are those of Chepil (11) and Young (12). Chepil (11) measured the lift and drag on a hemisphere which was placed on a plane wall. The hemisphere was 3 diameters downstream from a similar hemisphere. He found that $C_L \approx C_D$ and that each coefficient was of the order of magnitude of 0.1. The Reynolds numbers of Chepil's experiments were large varying from 5 (10^3) to 7.3 (10^4). Young (12) placed a sphere in a smooth, circular, inclined pipe. He adjusted both slope and discharge until the sphere was stationary but lifted slightly from the wall. Coefficient of lift and drag were computed. The ratio C_L/C_D was found to be about 1/2. In Young's experiments, the entire flow within the pipe was laminar. The Reynolds number was small. Thus

$$\frac{C_L}{C_D} = k_2 = k_2(R_d) \tag{12}$$

Introducing the above approximations into equation (9)

$$k_1 = \frac{4}{3}\sqrt{1 + k_2}\ C_D \frac{V_d^2}{(s-1)gd} \tag{13}$$

Solving for C_D

$$C_D = \frac{3k_1}{4\sqrt{1 + k_2}} \Big/ F_{sd}^2 \tag{14}$$

in which F_{sd}^* is $V_d / \sqrt{(s-1)gd}$. The unknown coefficients k_1 and k_2 may be approximated by

$$k_1 \approx \frac{1}{2}$$

and

$$k_2 \approx 1$$

Values of C_D computed from experimental results using equation (14) and the assumed values of k_1 and k_2 are shown in Figure 6 as a function of the Reynolds number $V_d d/\nu$.

The relationship between the coefficient of drag, C_D, and the Reynolds number as shown in Figure 6 is comparable to the results of Young (12) which are also shown in Figure 6. Even though the current study and Young's experiments are far from identical the values of C_D obtained are of the same order of magnitude. On the basis of his limited experiments Young decided that C_D was proportional to $R_d^{-1/3}$. The results of the current experiment can be represented by the function

$$C_D = 5.3 / \sqrt{R_d} \tag{15}$$

---

*Since the quantity F_{sd} is the ratio of the inertia forces to the gravity forces, this ratio can be considered as a sediment Froude number.

as shown in Figure 6.

The incipient-motion condition for the movement of particles in a laminar sublayer can be summarized by substituting equation (15) into equation (14) and solving for the sediment Froude number. Performing these operations

$$\mathbb{F}_{sdc} = \frac{2R_d^{1/4}}{9} \tag{16}$$

in which $\mathbb{F}_{sdc}$ is the value of the sediment Froude number at the incipient-motion conditions.

Incipient Motion (Scour Hole)

Motion of particles in the bottom of the scour hole is undoubtedly the result of the same forces that were discussed in the previous section. In fact the analysis through equation (9) is identical in the two cases.

The reference velocity, V, to be used in equation (9) should be the velocity V_d at the top of the particles as used in the previous analysis. Consider the flow pattern within the scour hole as shown in Figure 7. The vortex within the scour hole is maintained by the apparent shear stress at the interfacial region of the vortex and the main flow. This vortex is similar to a rotational vortex which is generated as a pail of water is rotated about the vertical axis. In the steady state the fluid velocity at the periphery will be the same as the wall of the pail. Utilizing this analogy the reference velocity V_d would be equal to the average main-flow velocity $\bar{V}$.

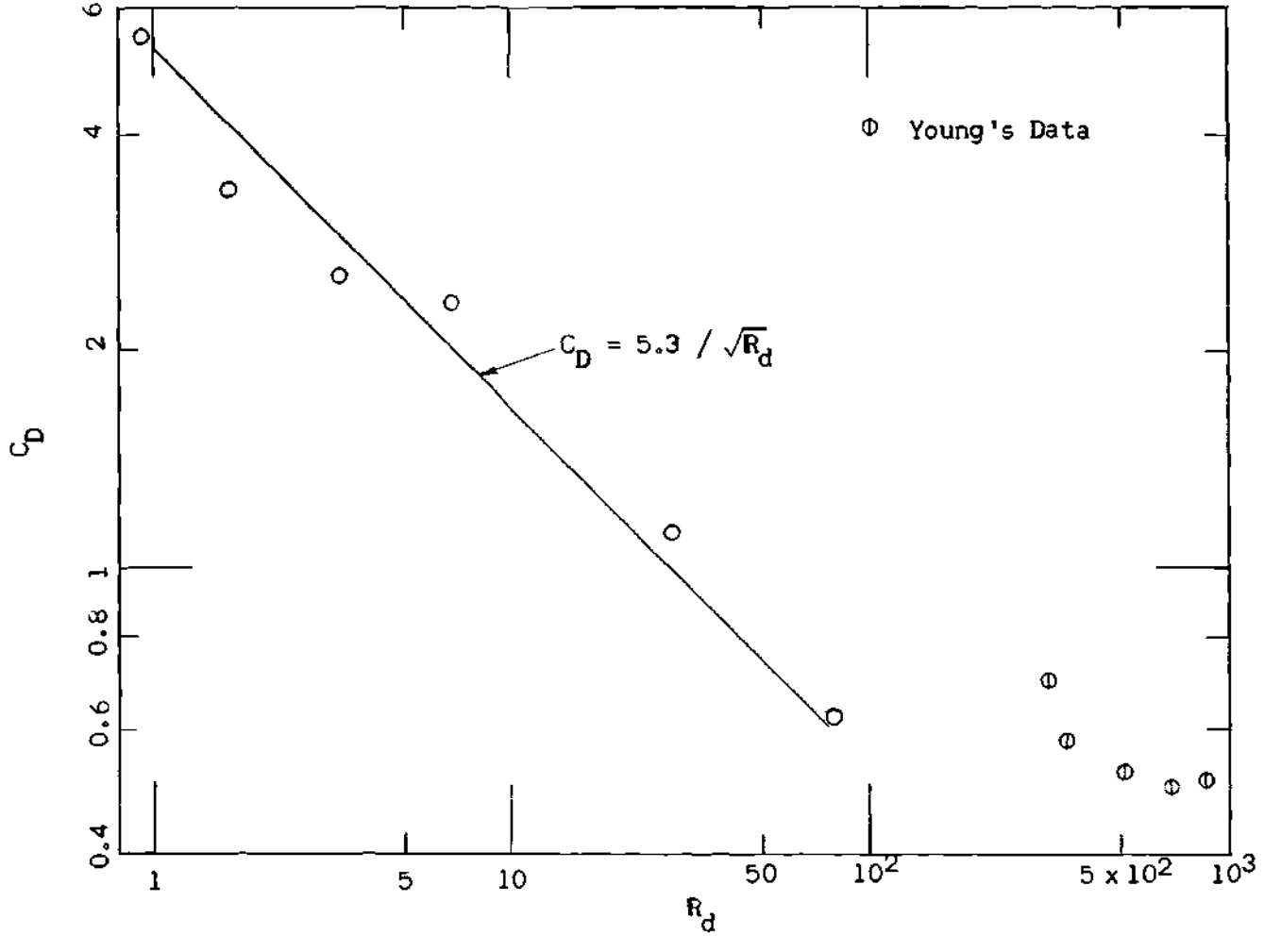

Figure 6. Variation of C_D with R_d at Incipient Motion (Plane Bed).

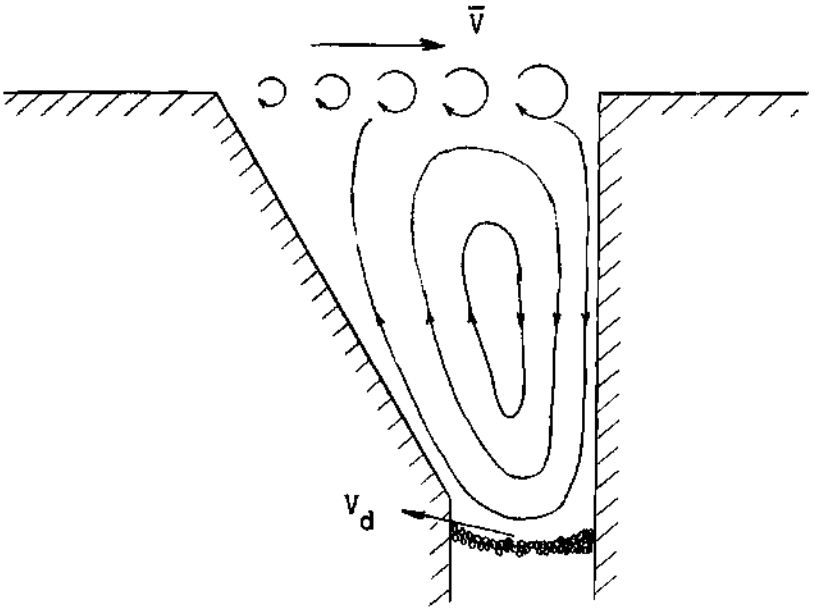

Figure 7. Scour-Hole Vortex Flow Pattern.

The lever-arm ratio, n_2/n_1 would be approximately equal to that discussed previously, that is $n_2/n_1 \cong 1/2$.

Likewise the approximations concerning the coefficients of lift and drag are applicable also to the scour-hole situation.

Values of C_D computed from experimental results using equation (14) are shown in Figure 8.

The relationship between the coefficient of drag, C_D, and the Reynolds number, R_d, as shown on Figure 8 can be approximated by

$$C_D = \text{constant} \tag{17}$$

This form of relationship for the coefficient of drag for the higher Reynolds numbers associated with this situation is not surprising. A similar situation holds for the coefficient of drag on a single sphere

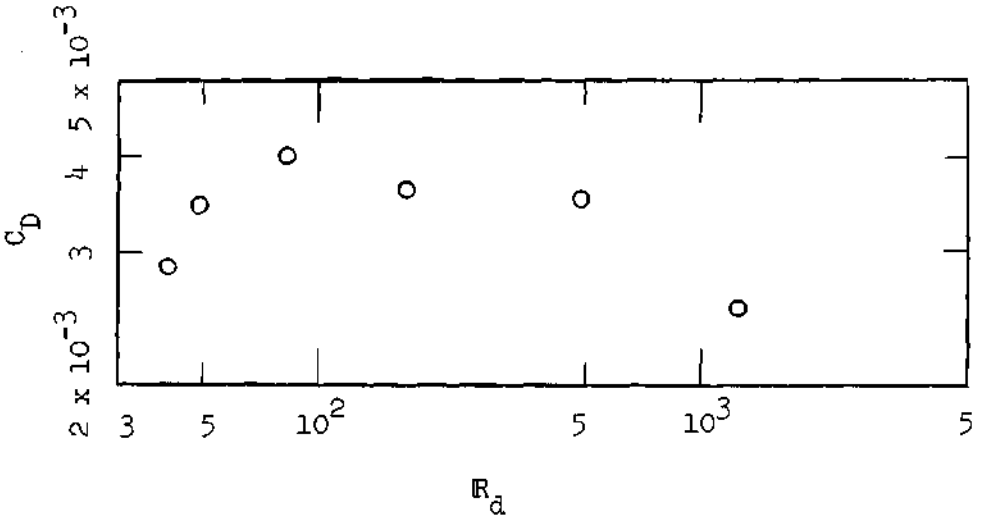

Figure 8. Variation of C_D with R_d at Incipient Motion (Scour Hole).

in an infinite fluid at high Reynolds numbers as shown by Rouse (13). The magnitude of C_D as computed by equation (14) appears to be too low by about one order of magnitude. The writer can think of no rational explanation for this discrepancy. Nevertheless, the form of the relationship is verified when the rate of transport from the scour hole data is correlated on the assumption that the coefficient of drag is a constant.

The incipient-motion condition for the movement of particles at the bottom of the scour hole can be summarized by substituting equation (17) into equation (14) and solving for the sediment Froude number. Performing these operations

$$F_{sdc} \cong 9.0 \tag{18}$$

in which F_{sdc} is the value of the sediment Froude number at the

incipient-motion conditions.

Sediment-Transport Rate (Plane Bed)

The rational analysis of sediment-transport rate follows directly from the analysis of the incipient-motion condition. The sediment-transport rate, Q_s, is assumed to be a function of the external forces on a typical sediment particle. Thus from equation (13)

$$Q_s = \varphi \left[C_D F_{sd}^2 \right] \tag{19}$$

in which Q_s is the volumetric rate of sediment transport.

The lefthand side of equation (19) can be non-dimensionalized by dividing Q_s by some significant reference discharge. The flow of fluid which is pertinent to the sediment-transport mechanism is only that flow near the sediment bed. Such a flow can be represented by the discharge due to a velocity V_d and a flow cross section of the height d from the wall times the width b of the bed. That is,

$$\frac{Q_s}{V_d db} = \varphi \left(C_D F_{sd}^2 \right) \tag{20}$$

in which b is the width of the sediment bed.

The relationship between the coefficient of drag, C_D, and the Reynolds number, R_d, as given by equation (15) is applicable to this condition of sediment transport because the ranges of Reynolds numbers are essentially similar. Substituting equation (15) into equation (20) yields

$$\frac{Q_s}{V_d db} = \varphi \left[\frac{F_{sd}^2}{\sqrt{R_d}} \right] \tag{21}$$

The variation of $Q_s/V_d db$ with $F_{sd}^2/\sqrt{R_d}$ is shown in Figure 9. This correlation encompasses the full range of sediment properties tested. That is, a size range from 0.106 mm to 0.585 mm. and a specific gravity range from 1.20 to 8.75.

Sediment Transport Rate (Scour Hole)

Several different mechanisms are required to produce transport out of the idealized scour hole, Figure 3. The local velocities at the sediment-water interface must be large enough to dislodge particles from the interface and entrain them in the flow. Once entrained, the particles follow the motion of the eddy in an upward direction. If the velocities in this upward flow of the eddy are insufficient to carry the sediment particles to the shear interface with the main flow, the particles will fall back to the bottom of the scour hole. These two mechanisms of entrainment and uplift must act in series to produce transport. Thus the rate of transport could be limited by either or both of them. During most test runs it was observed that no sediment, scoured from the sediment-water interface, returned to the scour area. An individual particle might settle momentarily on the 60 degree slope or be carried around in the eddy for several loops, but eventually the particle escaped the hole. Thus the eddy currents were able to carry sediment out of the hole at the same rate as they were entrained once the concentration of sediment in the eddy and on the 60 degree slope reached an equilibrium condition. During some runs a small amount of the sediment, which settled on the 60 degree slope, slid back into the scour area. This amount was quite small, however, compared to the overall rate of transport out of the hole. Thus it appears that the entrainment mechanism was the limiting mechanism.

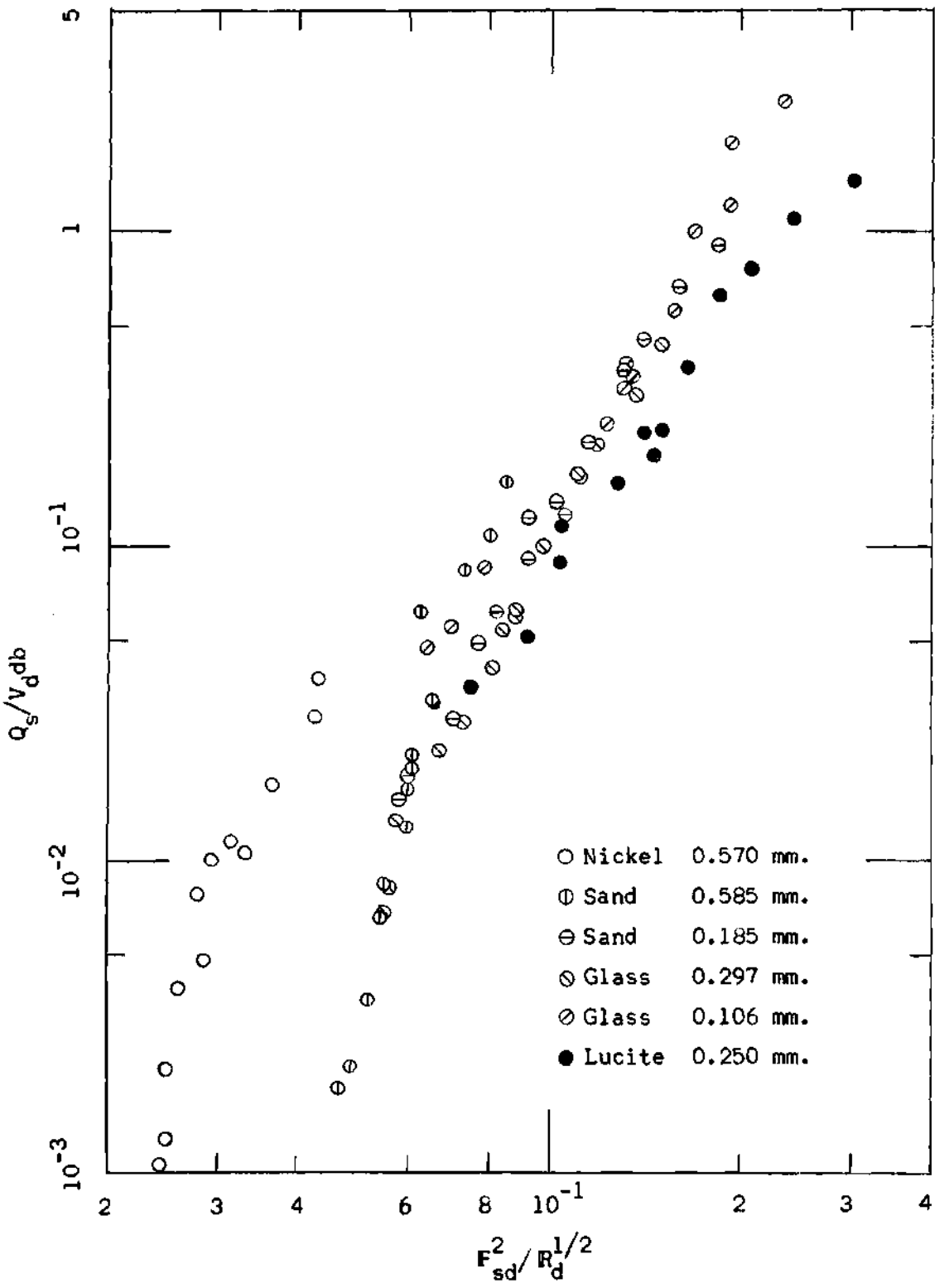

Figure 9. Variation of $Q_s/V_d db$ with $F_{sd}^2/R_d^{1/2}$ (Plane Bed).

The rate of entrainment at the sediment-water interface at the bottom of the scour hole is the same as the mechanism of sediment transport from a plane bed. Thus, if the rate of sediment transport out of the scour hole is limited by the entrainment mechanism then equation (20) is valid. Using the rotational vortex analogy for the fluid motion in the scour hole, the mean-flow velocity $\bar{V}$ was deemed to be the logical reference velocity. Thus equation (20) can be written

$$\frac{Q_s}{\bar{V}db} = \varphi\ (C_D\ F_{sd}^2) \tag{22}$$

From equation (17) the coefficient of drag, C_D, is a constant in the range of Reynolds numbers associated with sediment transport out of the scour hole. Thus equation (22) can be written

$$\frac{Q_s}{\bar{V}db} = \varphi\ (F_{sd}) \tag{23}$$

The variation of $Q_s/\bar{V}db$ with F_{sd} is shown in Figure 10. This correlation encompasses the full range of sediment properties tested. That is, a size range from 0.106 mm to 0.585 mm and a specific gravity range from 1.20 to 8.75.

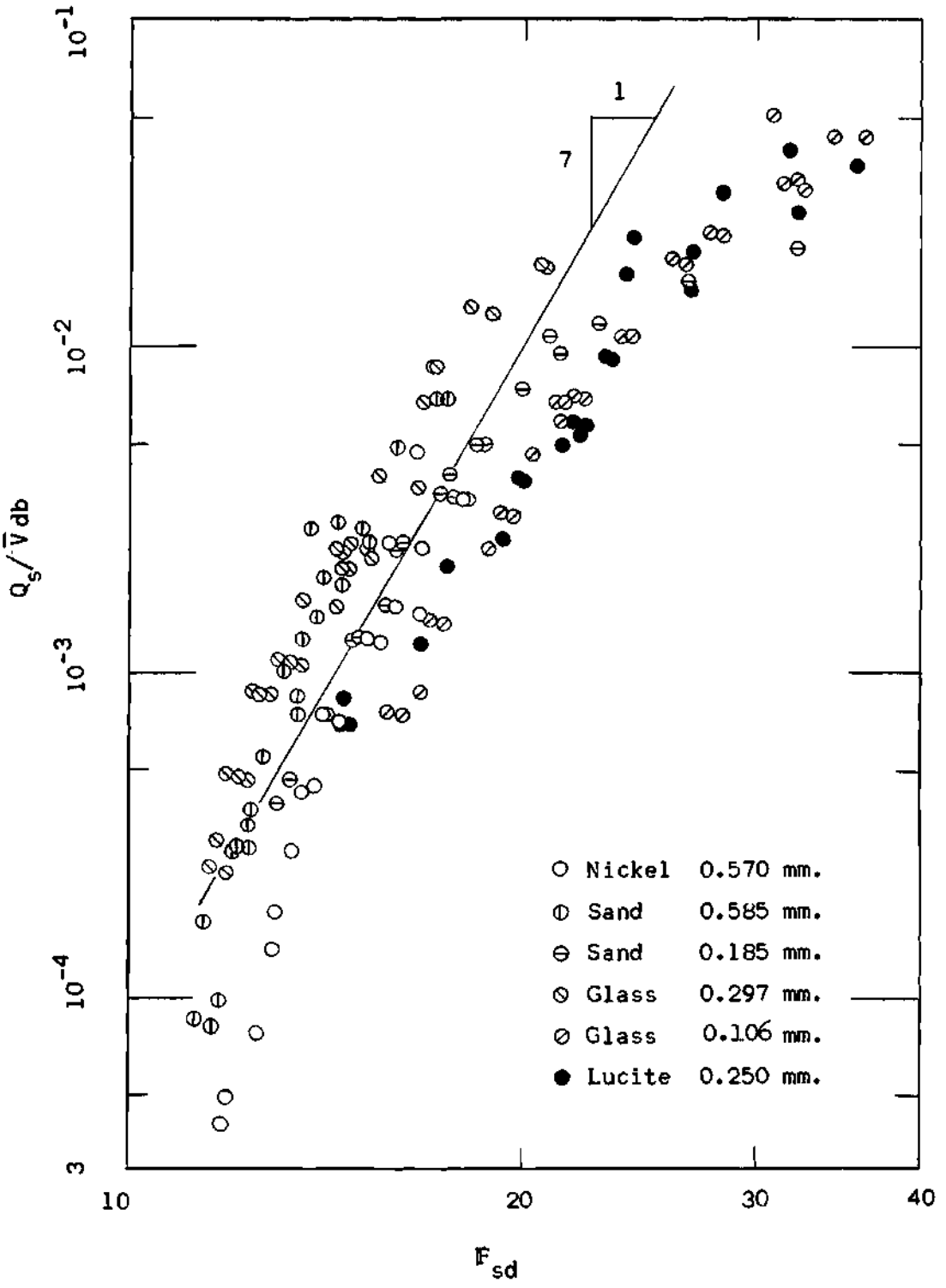

Figure 10. Variation of $Q_s/\bar{V}db$ with F_{sd} (Scour Hole).

CHAPTER V

DISCUSSION OF RESULTS

The results of this investigation demonstrate that a rational analysis of sediment transport is possible based upon the forces on a typical particle rather than an average shear stress over the bed. This approach to the analysis of sediment-transport phenomenon is a distinct departure from previous studies.

Incipient Motion

A particle begins to roll from the recess in the bed when the surface forces resulting from flow over the particle exceed the gravity force tending to resist the movement. Traditionally the surface forces are assumed to be proportional to the boundary shear stress, that is

$$\text{surface force} \propto \tau_o d^2$$

The resisting force is proportional to the gravity force, that is,

$$\text{resisting force} \propto (\gamma_s - \gamma) d^3$$

Shields (3) reasoned that motion is incipient when the surface force, $\tau_o d^2$, reaches a critical value, that is, when $\tau_o = \tau_c$. The force ratio at incipient motion is proportional to the Shields' parameter $\tau_c/(\gamma_s - \gamma)d$. In addition, Shields reasoned that the value of the incipient-motion parameter would be a function of the ratio of the particle diameter, to the laminar sublayer thickness d/δ'. From experimental

studies of velocity distribution over smooth boundaries the thickness of the laminar sublayer has been selected as being $\delta' = 11.6\nu/u_*$. Hence d/δ' is proportional to u_*d/ν. The well known Shields' diagram is a graph of experimentally determined values of $\tau_c/(\gamma_s - \gamma)d$ as a function of u_*d/ν.

For particles immersed in a laminar boundary layer, Shields reasoned that

$$\frac{\tau_c}{(\gamma_s - \gamma)d} \propto \left[\frac{u_*d}{\nu}\right]^{-1} \tag{24}$$

The applicability of this formulation to the experimental results of this study is demonstrated in the following. The boundary shear stress, τ_o, is determined by the velocity gradient at the boundary and the viscosity, μ, of the fluid. For turbulent flow over a <u>smooth</u> boundary the velocity gradient at the boundary and throughout the laminar sublayer is given by

$$\frac{dv}{dy} = \frac{V_{\delta'}}{\delta'} \tag{25}$$

in which $V_{\delta'}$, is the velocity at the edge of the laminar sublayer, and δ' is the thickness of the laminar sublayer. Thus the boundary shear stress τ_o may be written

$$\tau_o = \mu \frac{dv}{dy} = \mu \frac{V_{\delta'}}{\delta'} \tag{26}$$

in which τ_o is the boundary shear stress, and μ is the absolute viscosity of the fluid.

The shear velocity, u_*, is defined by the boundary shear stress, τ_o, and the fluid density, ρ.

$$u_* = \sqrt{\tau_o/\rho} \tag{27}$$

in which u_* is the shear velocity, and ρ is the fluid density. Combining equation (26) and equation (27),

$$u_* = \sqrt{\nu \frac{V_{\delta'}}{\delta'}} \tag{28}$$

in which ν is the kinematic viscosity of the fluid.
The slope of the velocity profile in the laminar sublayer may be given by V_d/d when d is less than δ'. Thus

$$\frac{V_{\delta'}}{\delta'} = \frac{V_d}{d} \tag{29}$$

Substituting equation (29) into equation (28) and squaring both sides

$$u_*^2 = \frac{\nu V_d}{d} \tag{30}$$

The square of the shear Reynolds number, R_*, becomes

$$R_*^2 = \left[\frac{u_* d}{\nu}\right]^2 = \frac{\nu V_d}{d} \frac{d^2}{\nu^2} = \frac{V_d d}{\nu} = R_d \tag{31}$$

By substitution of equations (26) and (29) the Shields' parameter is

$$\frac{\tau_c}{(\gamma_s - \gamma)d} = \frac{\nu}{dV_d} \frac{V_d^2}{(s-1)gd} = \frac{F_{sdc}^2}{R_d} \tag{32}$$

Using equations (31) and (32) Shields' relationship given by equation (24) can be transformed into

$$\frac{F_{sdc}^2}{R_d} \propto \frac{1}{\sqrt{R_d}} \tag{33}$$

or

$$F_{sdc} \propto R_d^{1/4} \tag{34}$$

Since equation (34) is identical to equation (16), Shields implicitly employed the same assumption as the writer, namely, that $C_D \propto 1/\sqrt{R_d}$.

The interrelationship between the Shields diagram and the well established drag coefficient diagram shown by the above demonstration, can be used to hypothesize the shape of the low Reynolds number portion of the Shields diagram as shown in Figure 11. For creeping motion the coefficient of drag, C_D, is proportional to R_d^{-1}. Transformation of this proportionality to the Shields co-ordinates suggests that the Shields parameter, $\tau_c/(\gamma_s - \gamma)d$, is independent of R_* for creeping motion. Similarly the transformation of the relationship C_D = constant to the Shields coordinates suggests that

$$\tau_c/(\gamma_s - \gamma)d \propto \frac{1}{R_*^2}$$

for high values of R_*. Actually the transformation is not valid in the region of higher Reynolds number because the sediment particles project beyond the laminar layer and the linear velocity profile assumption inherent in the transformation is incorrect. Thus the observed

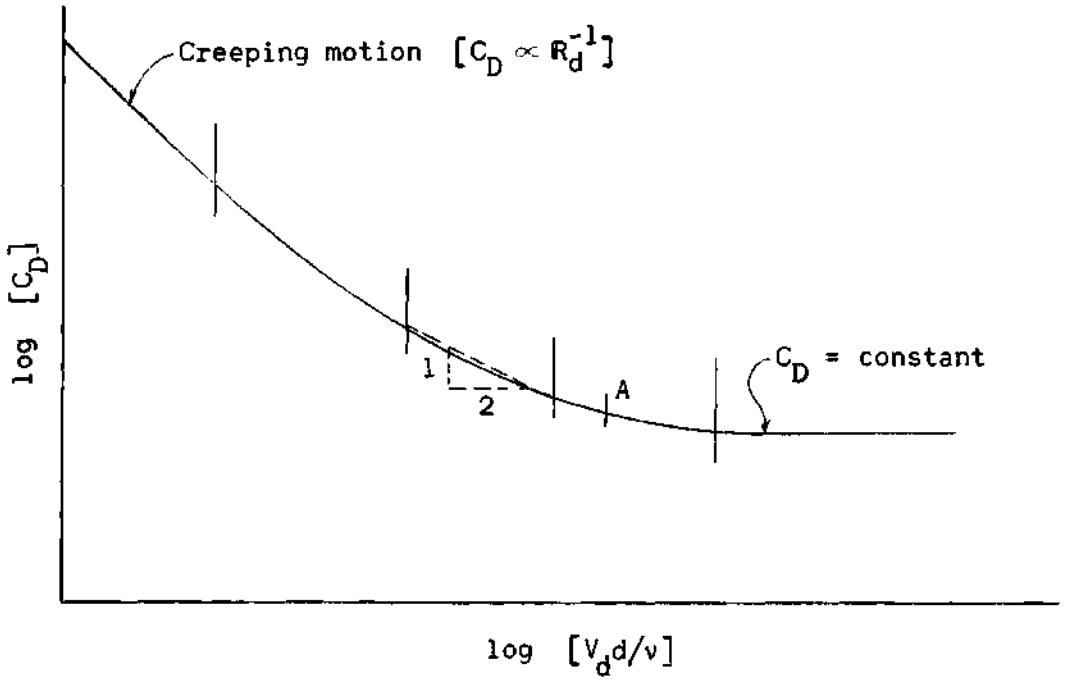

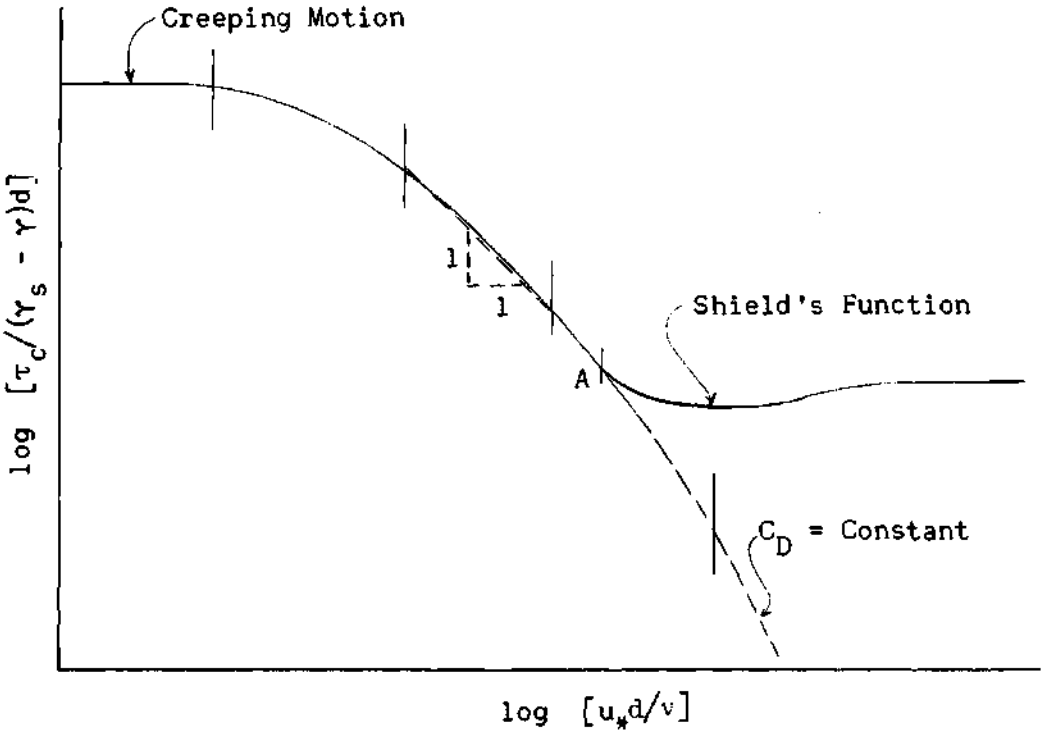

Figure 11. Suggested Form of Shields Diagram.

trend departs from the hypothetical curve at point A. Between the limiting conditions of $C_D \propto \frac{1}{R_d}$ and C_D = constant the drag coefficient diagram is a continuous curve of increasing slope. The transformation of this region to the Shields co-ordinates should be a continuous curve of decreasing slope. Following the functional relationship of equation (22) suggested by Shields, many writers have shown a straight line at a slope of minus one as the probable form of the Shields function at low Reynolds number. Such a linear form is but a linearized approximation to a portion of the continuous curve of this hypothesis. Equation (15) was just such an approximation to the drag coefficient curve. Figure 11 shows the conventional form of the drag coefficient diagram and the corresponding suggested form of the Shields diagram.

Evaluation of Widely-Used Transport Functions

Sediment-transport functions for two-dimensional flow are relations between the sediment-transport rate, q_s, and the boundary shear stress, τ_o. Garde (4) showed that all presently suggested sediment-transport functions could be put in the form

$$\frac{q_s}{u_* d} = \varphi \left[\frac{\tau_o}{(\gamma_s - \gamma)d} \right] \tag{35}$$

in which q_s is the volumetric rate of sediment transport per unit width, u_* is the shear velocity, and τ_o is the shear stress at the boundary. Garde demonstrated that a good correlation of plane-bed data from many previous investigations is obtained by using the two parameters $q_s/u_* d$ and $\tau_o/(\gamma_s - \gamma)d$.

The right hand side of equation (35) can be transformed into a sediment Froude number form by the substitution from equation (27) of $\tau_o = u_*^2 \rho$. That is,

$$\frac{q_s}{u_* d} = \varphi \left[\frac{u_*^2}{(s-1)gd} \right] \tag{36}$$

In this form, equation (36) is substantially the same as equation (20) of Chapter V with C_D = constant and $V_d = u_*$.

The choice of u_* for the reference velocity in the test data reported by Garde is justified because in each case the sediment particles protruded beyond the laminar sublayer and into the turbulent flow. In this case the local velocity V_k a distance k from the boundary is given by Rouse (14) as

$$V_k = 8.5\, u_* \tag{37}$$

as determined from Nikuradse's (15) sand roughness tests in which k was the sand grain diameter. Thus the reference velocity V_k is a linear function of the shear velocity u_*.

The local Reynolds number, R_d, as given by equation (11) of Chapter IV can be written in terms of the shear velocity u_*. That is

$$R_* = \frac{u_* d}{\nu} \tag{38}$$

in which R_* is referred to as the shear Reynolds number. This Reynolds number is related to the Reynolds number R_d by equation (31). All of the data reported by previous investigators was in a Reynolds number

range ($R_d > 3900$). Thus the coefficient of drag, C_D, would be nearly constant.

The two-parameter transport functions used by previous investigators produced a good correlation of the reported data, only, because the drag coefficient was essentially constant over the range of Reynolds numbers represented by these data. Thus the two-parameter function is but a special case of the more general relationship given by equation (20) of Chapter IV.

The inability of a two-parameter relationship to correlate the data of this investigation is apparent from Figure 12. The reason must be that the particles were immersed in a well behaved, laminar boundary layer. In such a situation the linear velocity profile near the boundary requires a constant shear stress in this region. If the variation of particle diameter occurred in this same region the force analysis based on average boundary shear would require the same force on a variety of different grain diameters. Thus, for particles immersed in a laminar boundary layer the additional parameter of Reynolds number must be included in the analysis.

Saturation of the Scour-Hole Sediment-Transport Mechanism

The scour hole data as plotted on Figure 10 show a tendency for Q_s to become less sensitive to increase in F_{sd} for high values of F_{sd}. This suggests some kind of saturation of the mechanism. A possible explanation of this effect would be as follows:

When a sediment particle is carried to the interface between the main flow and the eddy it must be accelerated with a corresponding loss of momentum in the main flow. As the rate of transfer of sediment

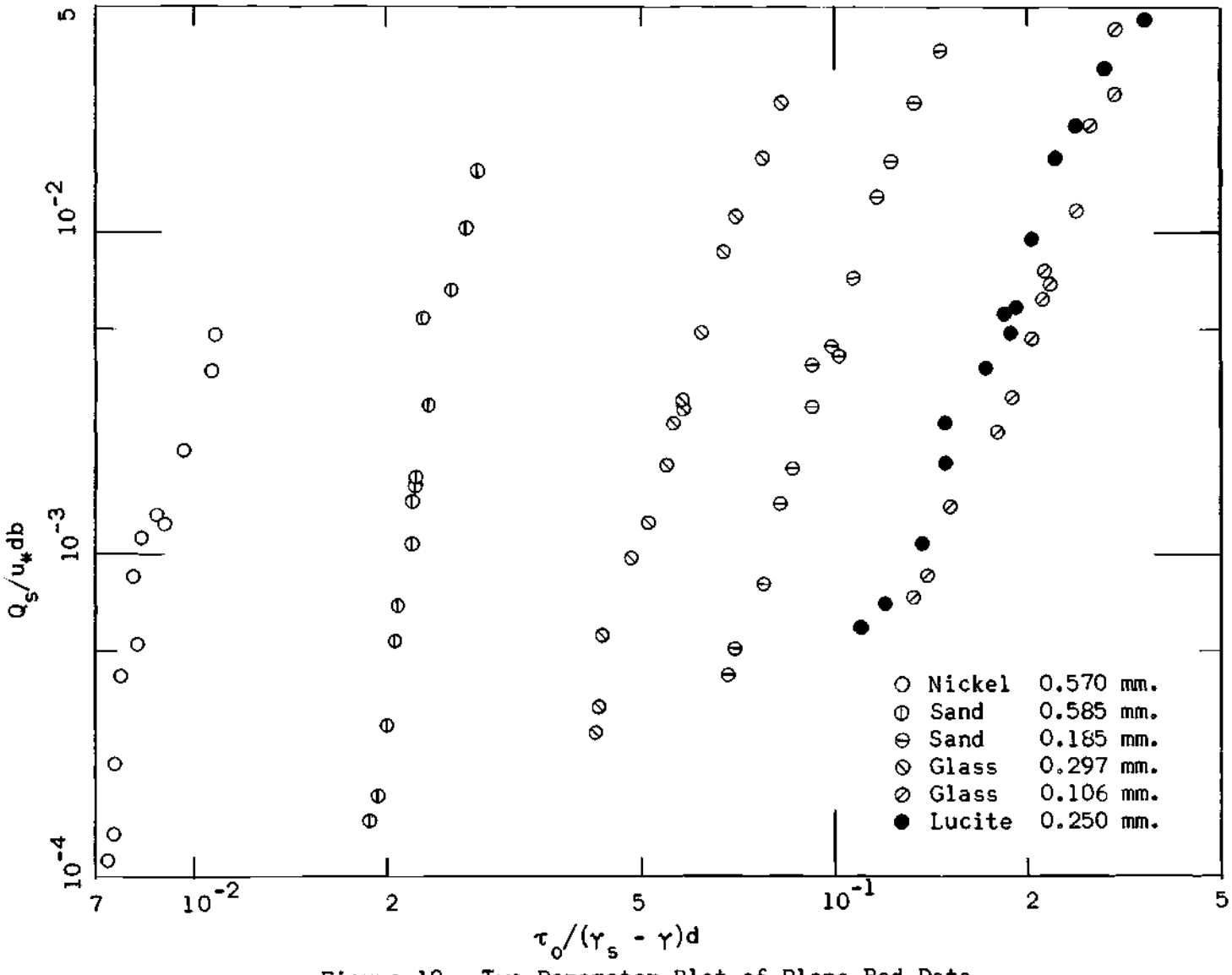

Figure 12. Two Parameter Plot of Plane-Bed Data.

particles to the main flow becomes large the reduction in momentum is sufficient to slow down the main eddy which must derive its energy by momentum transfer from the main flow. At low transport rates this effect would be almost negligible.

Reanalysis of Rouse's and Laursen's Data

Carstens,* in a yet unpublished reanalysis of Rouse's and Laursen's data, suggested that Q_s was a function of F_{sd}. The data reported by Rouse (6) and Laursen (7) showed the progressive change of scour boundary with time. Carstens used this reported data to determine the rate of sediment transport. From this analysis Carstens has concluded that the rate of sediment transport is proportional to the seventh power of the sediment Froude number. The results shown in Figure 10 indicate that the functional relationship between sediment transport rate and the sediment Froude number is more complicated than a seventh-power relation. In these experiments the seventh-power function is reasonable in the range $12 < F_{sd} < 22$ as shown on Figure 10. The sediment-transport rate is even more sensitive to changes in F_{sd} as F_{sd} approaches F_{sdc} (about 9). On the other hand, the results shown in Figure 10 show that the sediment-transport rate is less sensitive to changes in F_{sd} when $F_{sd} > 22$. In spite of these variations, Carstens' selection of $Q_s \propto F_{sd}^7$ is a reasonable approximation.

---

*Dr. M. R. Carstens, Professor of Civil Engineering, Georgia Institute of Technology showed these results to the writer.

CHAPTER VI

CONCLUSIONS

The most significant conclusion of this study is that the boundary-shear force is not a measure of the surface forces on individual particles which are submerged in a laminar boundary layer. For the flat bed immersed in a laminar boundary layer, the measured transport rate, Q_s, will not correlate with the boundary shear stress, τ_o. Correlation of the data can be achieved only by using the velocity in the vicinity of the particles. Surface forces upon the bed particles are proportional to the drag force given by the conventional drag relationship.

$$\text{Drag force} \propto C_D d^2 \frac{\rho V_d^2}{2}$$

in which C_D is a coefficient of drag, d is the particle diameter, ρ is the mass density of the fluid, and V_d is a reference velocity in the vicinity of the particle. The rate of sediment transport is proportional to the surface force upon the bed particles. Hence a transport function for bed particles submerged in a laminar boundary layer must involve the drag on the particles due to the local velocity V_d rather than the boundary-shear stress τ_o.

Incipient motion is the limiting condition of zero transport for the sediment-transport function. It follows from above therefore, that the criteria for incipient motion of particles submerged in a laminar

boundary layer should involve the drag on the particles due to the local velocity V_d, rather than the boundary shear stress τ_o.

Using the local velocity in the vicinity of the particles and the conventional relationship between drag coefficient and Reynolds number, the form of the Shields diagram can be predicted for that portion of the Shields diagram in which the bed particles are submerged in a laminar layer.

A non-dimensionalized sediment-transport function requires a reference discharge. The fluid flow involved in the transport mechanism is only that flow near the sediment-water interface. Such a flow can be formed from the local velocity V_d and the flow area within one grain diameter of the bed. Hence the sediment-transport function is

$$\frac{Q_s}{V_d db} \propto C_D \frac{V_d^2}{(s-1)gd}$$

in which Q_s is the rate of sediment transport, b is the width of the bed, C_D is the coefficient of drag, s is the specific gravity of the sediment material, and g is the acceleration due to gravity.

At high values of the local Reynolds number, $V_d d/\nu$, the coefficient of drag on bed particles becomes independent of the local Reynolds number.

For transport from the bottom of a scour hole the sediment-transport function is approximated by the power function

$$\frac{Q_s}{V_d db} \propto \left[\frac{V_d}{\sqrt{(s-1)gd}}\right]^7$$

APPENDIX A

BOUNDARY-LAYER ANALYSIS

Drag forces on bed particles must be related to the magnitude of fluid velocities in the neighborhood of the particles. In the analysis of data from the experiments with bed-load transport from a plane bed it was necessary to know what the velocities were in the neighborhood of the bed. This required a relationship between measured values of average velocity in the test section and local velocities near the bed. An approximate analysis assuming flat-plate conditions indicated that the particles were very probably immersed in a laminar boundary layer. The three-dimensional nature of the test section and elliptical contraction made a flat-plate analysis too much of an approximation. It was necessary therefore to measure the velocity profile existing in the apparatus at the beginning of the sediment bed.

Velocity Profile

In order to simplify the instrumentation air was used as the working fluid for this test. The test section was connected to a centrifugal blower. The upstream section of the six-inch pipe and the first elbow were retained in their original relationship to the test section. The sediment-supply tube was removed and replaced with a stagnation tube and traverse facility. The stagnation tube was mounted so that it could be removed entirely from the flow by lowering it into the supply-tube opening. The location of the tube relative to the wall of the test section

was measured externally by observing the position of a reference point on the stem of the tube with a cathometer. The stagnation tube was 0.0275 in. O.D. and 0.0160 in. I.D. The static pressure was measured from an opening in the top of the test section directly above the stagnation tube. The pressure difference between static and dynamic probes was measured by a micromanometer with water as the manometric fluid. The general arrangement of the apparatus is shown in Figure 13.

The velocity profile along a vertical diameter of the test section was measured for two different discharges. These profiles are shown on Figure 14. They indicate the presence of a boundary layer. Schlichting (16) presents a similarity solution for the laminar boundary layer along a flat plate. Following the method of Blasius (17) a dimensionless profile is plotted by using the coordinates of

$$\frac{u}{U_\infty} = \varphi\left[y\sqrt{\frac{U_\infty}{\nu X}}\right] \tag{39}$$

where u is the velocity at a distance y from the boundary

U_∞ is the velocity an infinite distance from the boundary

ν is the kinematic viscosity

X is the distance from the start of boundary-layer growth to the section in question

The flow near the boundary of the test section in this investigation can be considered two dimensional. Therefore, the velocity profile data in the vicinity of the boundary for both discharges was plotted as for a flat plate. Since the cross section of interest was a fixed distance X from the beginning of boundary-layer growth, the exact

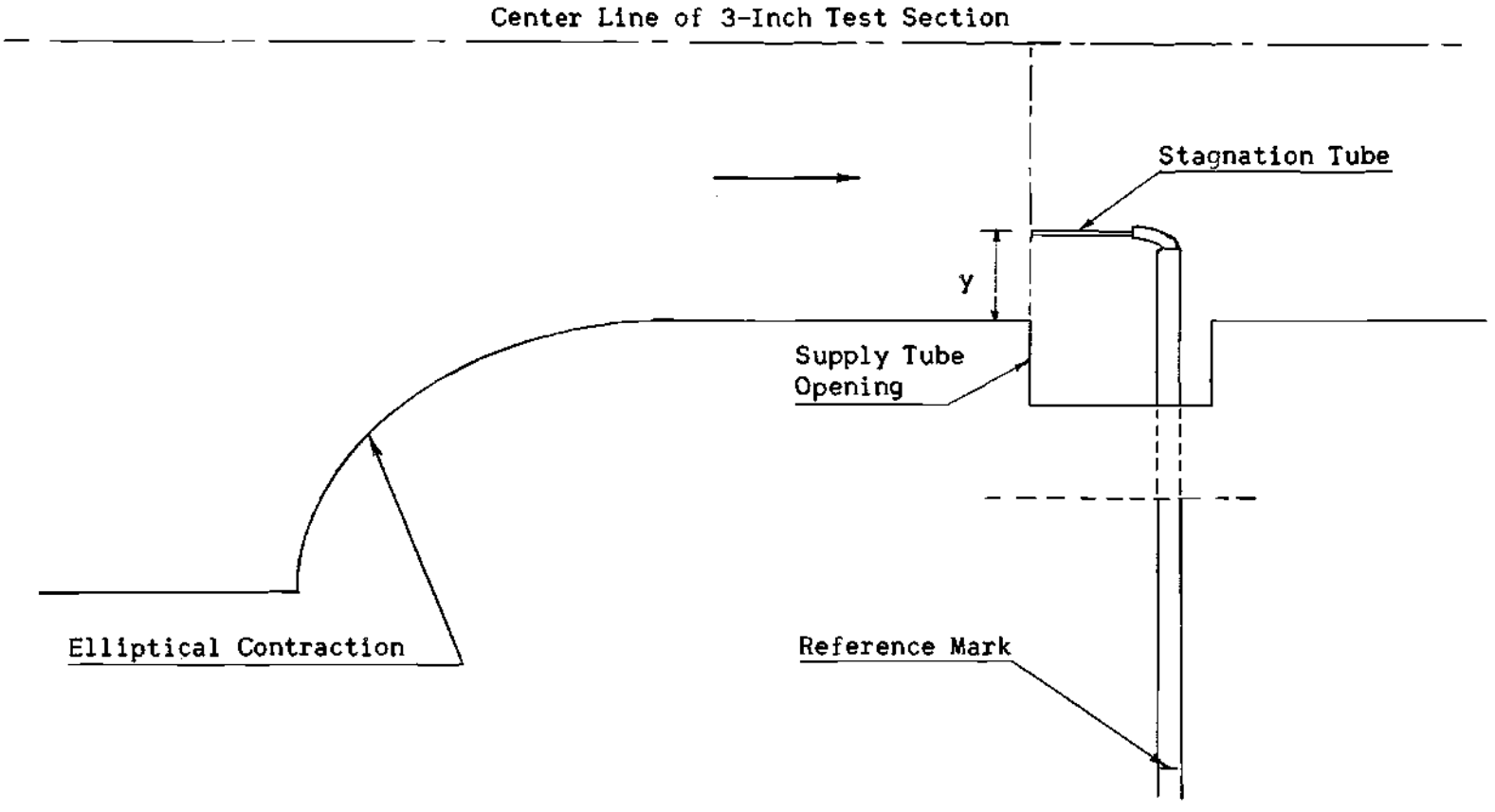

Figure 13. Velocity Profile Apparatus.

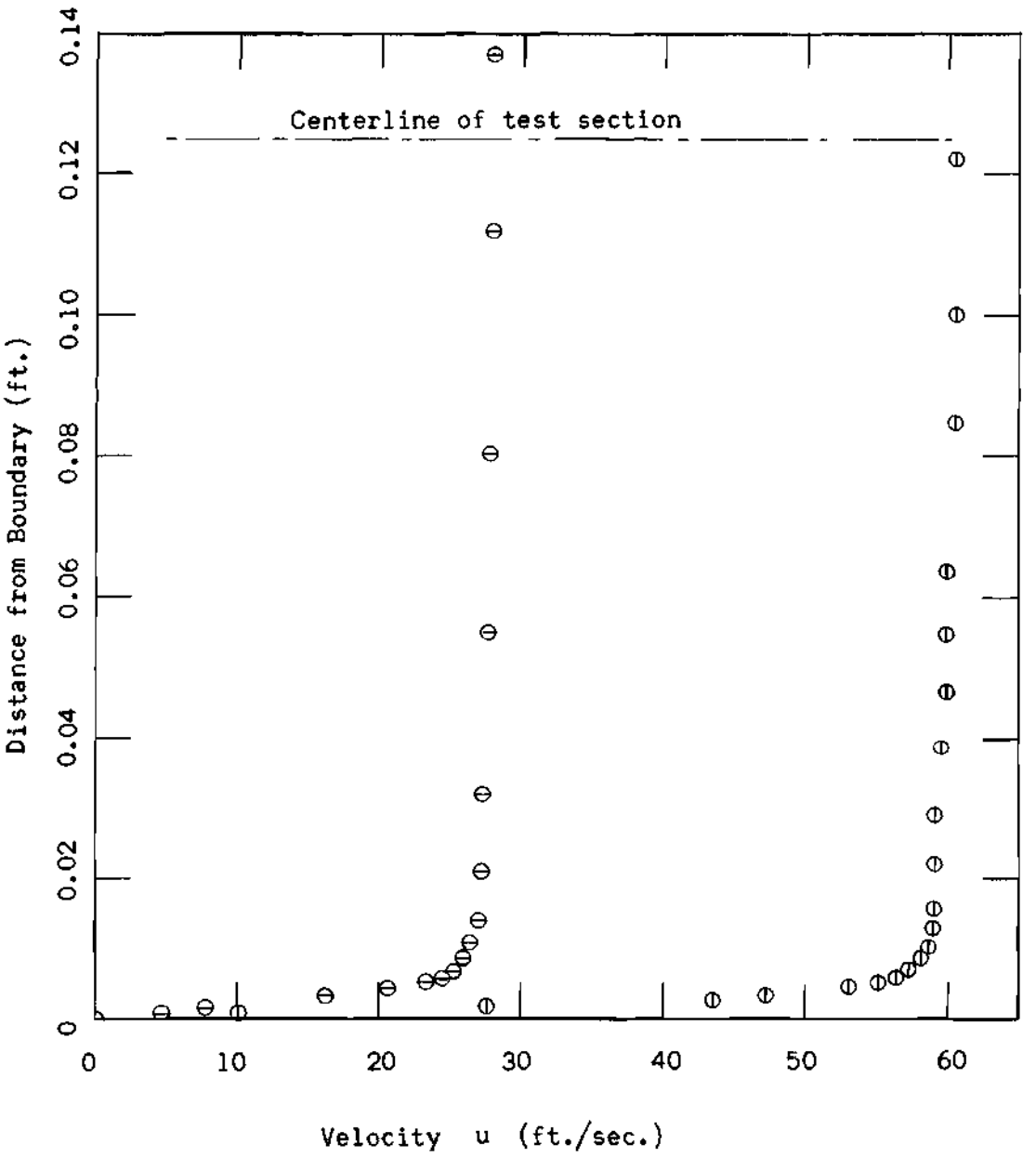

Figure 14. Velocity Profiles.

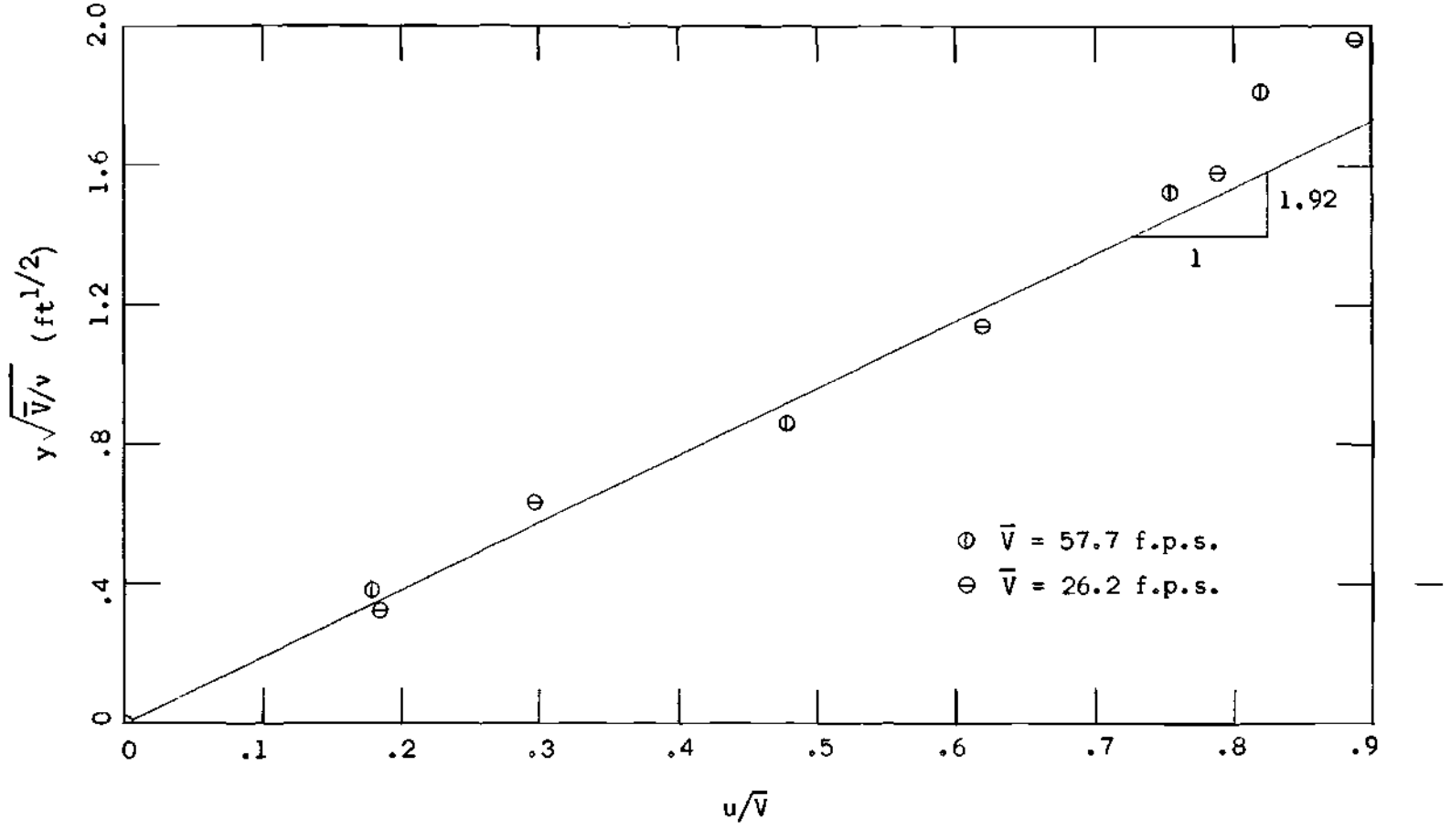

Figure 15. Boundary Layer Profile.

value of X was immaterial at this stage and was omitted in Figure 15. The average velocity $\bar{V}$ was substituted for U_∞ because such a velocity does not exist in closed conduit flow.

Figure 15 shows that for data points in the range $0 < \frac{u}{\bar{V}} < 0.7$, these data plot as a single linear relationship common to both discharges. Thus

$$y \sqrt{\frac{\bar{V}}{\nu}} = m \frac{u}{\bar{V}} \quad (\text{feet})^{1/2} \tag{40}$$

where m is the slope of the line

or

$$u = \frac{\bar{V}}{m} y \sqrt{\frac{\bar{V}}{\nu}} = \frac{1}{m} y \frac{\bar{V}^{3/2}}{\nu^{1/2}} \quad \text{feet per second} \tag{41}$$

The velocity a distance d from the boundary was assumed to be the significant local velocity. From equation (41) this local velocity V_d is

$$V_d = \frac{1}{m} \frac{dV^{3/2}}{\nu^{1/2}} \quad \text{feet per second} \tag{42}$$

From Figure 15 the slope m is 1.92. Thus,

$$V_d = \frac{1}{1.92} \frac{dV^{3/2}}{\nu^{1/2}} \quad \text{feet per second} \tag{43}$$

Equivalent Length of Flat Plate

The velocity profile near the boundary can be compared to the laminar boundary layer on a flat plate at some distance X_e from the

leading edge of the plate. The velocity profile as shown in Figure 15 is essentially linear for $(0 < \frac{u}{V} < 0.7)$. The Blasius (17) profile also is nearly linear for $(0 < \frac{u}{U_\infty} < 0.6)$. Thus, the profiles shown in Figure 15 can be described in relation to the Blasius profile a distance X_e from the edge of the plate. Schlichting (16) shows the variation of u/U_∞ with $y\sqrt{U_\infty/\nu X}$ for the laminar boundary layer on a flat plate. For $(0 < \frac{u}{U_\infty} < 0.5)$ this curve can be approximated by a straight line of slope 1/3. That is,

$$\frac{u}{U_\infty} = \frac{1}{3} y\sqrt{\frac{U_\infty}{\nu X}} \tag{44}$$

Comparing equation (44) with equation (40) and solving for X yields

$$X = \left(\frac{1.92}{3.00}\right)^2 = 0.41 \text{ ft.}$$

or

$$X_e = 0.41 \text{ ft.}$$

in which X_e is the equivalent length of flat plate.

The boundary layer can be described by analogy with the Blasius profile with X equal to X_e. The displacement thickness δ^* is given by Schlichting (18) as

$$\delta^* = 1.72\sqrt{\frac{\nu X}{V}} \tag{45}$$

in which δ^* is the boundary-layer displacement thickness as defined by Schlichting (19).

Substituting the value of X_e

$$\delta^* = 1.10\sqrt{\frac{\nu}{\bar{V}}} \qquad (46)$$

The foregoing analysis is based on the assumption that the boundary layer shown in Figure 14 is laminar. A laminar boundary-layer velocity profile is distinguished by the similarity of the velocity profile to the Blasius (17) profile. In this case, similarity between tests at two different discharges was demonstrated in Figure 15. A comparison with the Blasius profile suggested that the boundary layer in these tests was equivalent to the boundary layer on a flat plate at a distance of 0.41 feet from the beginning of boundary layer growth. The velocity-profile section was located two inches downstream from the end of a two inch by one and one half inch elliptical contraction. Thus 0.41 feet of flat plate is a reasonable substitute for the actual distance over which the boundary layer developed. The criteria for the beginning of transition from a laminar to a turbulent boundary layer on a flat plate is given by Schlichting (20) as

$$\frac{U_\infty X_c}{\nu} = 3.5 \times 10^5 \text{ to } 10^6 \qquad (47)$$

in which U_∞ is the velocity an infinite distance above the plate, and X_c is the distance from the beginning of boundary-layer growth. Replacing U_∞ by the maximum average velocity $\bar{V}$ which occurred in these tests and solving for X_c

$$X_c = 1.78 \text{ feet}$$

in which X_c is the distance to the beginning of transition from a laminar to a turbulent boundary layer. In these tests X_c was always greater than X, hence the boundary layer was laminar at the start of the sediment bed. The influence of distributed roughness on transition was measured by Feindt (21). He showed the variation of $\bar{V}X_c/\nu$ with $\bar{V}d/\nu$. On the basis of this study the distance X_c to the beginning of transition for these tests is

$$X_c = 0.508 \text{ feet}$$

Since the sediment bed was only one inch long it appears that the boundary layer was laminar over the entire bed.

The analysis of Chapter IV assumed that the velocity profile in the vicinity of the particle was linear. This condition is closely approximated in the laminar boundary layer for $y < \delta^*$. Thus, the linear velocity profile assumption of Chapter IV is confirmed if $d/\delta^* < 1$. Table 29 shows the range of d/δ^* for each series of plane-bed tests.

APPENDIX B

SEDIMENT PROPERTIES

Measurement of Porosity

The sediment supply mechanism provided a very accurate measure of the rate of piston displacement. The quantity of interest was, however, the volumetric rate of supply of the sediment particles themselves. The displacement in the supply tube included sediment particles plus the water-filled voids between the particles. Thus, the true rate of sediment discharge could be determined only if the porosity of the sediment, as it existed in the supply tube, could be determined.

The porosity is the volume of voids divided by the total volume. It was measured experimentally by the following procedure. The test section was removed from above the supply tube and replaced by a plexiglass container as shown in Figure 16. The dish and supply tube was filled with water and sediment was poured into the tube. The sediment fell through the water and settled in the tube in the same manner as in a test run. The tube was tapped lightly to give a similar compaction. The water above the end of the supply tube was then drained off and the excess sediment above the end of the tube was screeded off. A known volume of sediment-water mixture was forced out of the top of the tube by turning the drive mechanism a known number of revolutions by hand. Surface tension held the displaced sediment together long enough to scrape it into an evaporating dish. This sample was dried in an oven overnight. The volume of sediment displaced was determined by dividing

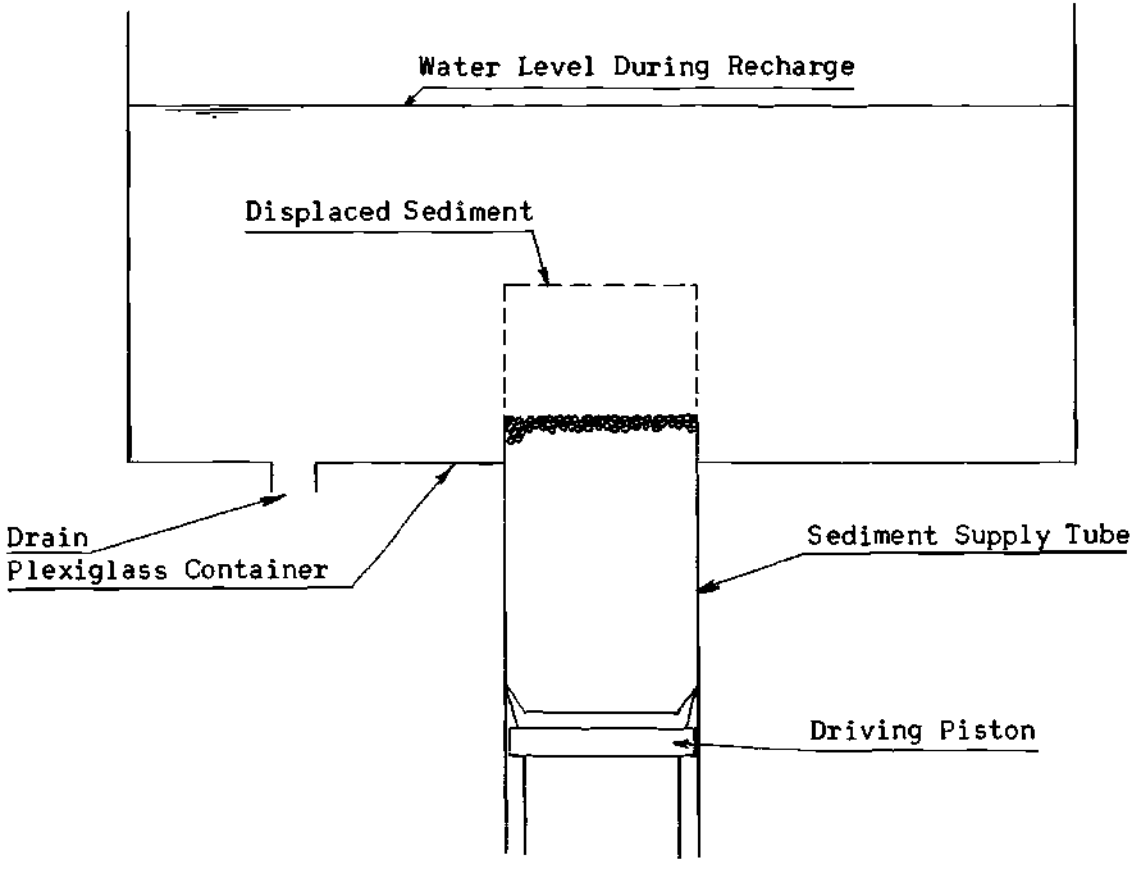

Figure 16. Porosity Apparatus.

the dry weight of the sample by the specific weight of the sediment material. The porosity was then determined from the known displacement and volume of sediment.

$$\text{Porosity} = \frac{\text{displaced volume} - \text{volume of sediment}}{\text{displaced volume}}$$

The above procedure was repeated several times for each sediment.

In some of the early runs the sediment was allowed to settle undisturbed during the recharging process. In later runs an attempt was made to produce more uniform porosity by tapping the side of the supply tube during recharging. In order to determine the effect of this tapping on the porosity, the sediments used in the earlier runs were tested for both methods of recharging. As can be seen in Table 22 the tapping had a measurable effect on the porosity. The rate of sediment supply was determined for each run by multiplying the rate of piston displacement by one minus the porosity for that sediment according to the method of recharge which had been used.

Sieve Analysis

The mean diameter of each sediment was determined from a sieve analysis using U. S. Standard Sieves. The analyses of both sands and the larger glass beads were performed under the direction of Dr. M. R. Carstens for an earlier study. The analyses of the smaller glass beads, the nickel and the Lucite were performed by the writer. The data from all analyses are shown in Tables 15 to 20 inclusive. The mean diameter was determined graphically from a plot of the analysis data on log-probability coordinates as shown in Figure 17.

Specific Gravity Analysis

The specific gravity of the glass and sand sediments was determined by a standard procedure as outlined in ASTM. The nickel was very nearly chemically pure so that the published value of 8.75 was used for this material. The manufacturer's value of 1.20 for the specific gravity of Lucite was accepted as it was felt that standard testing procedures would be uncertain with this material.

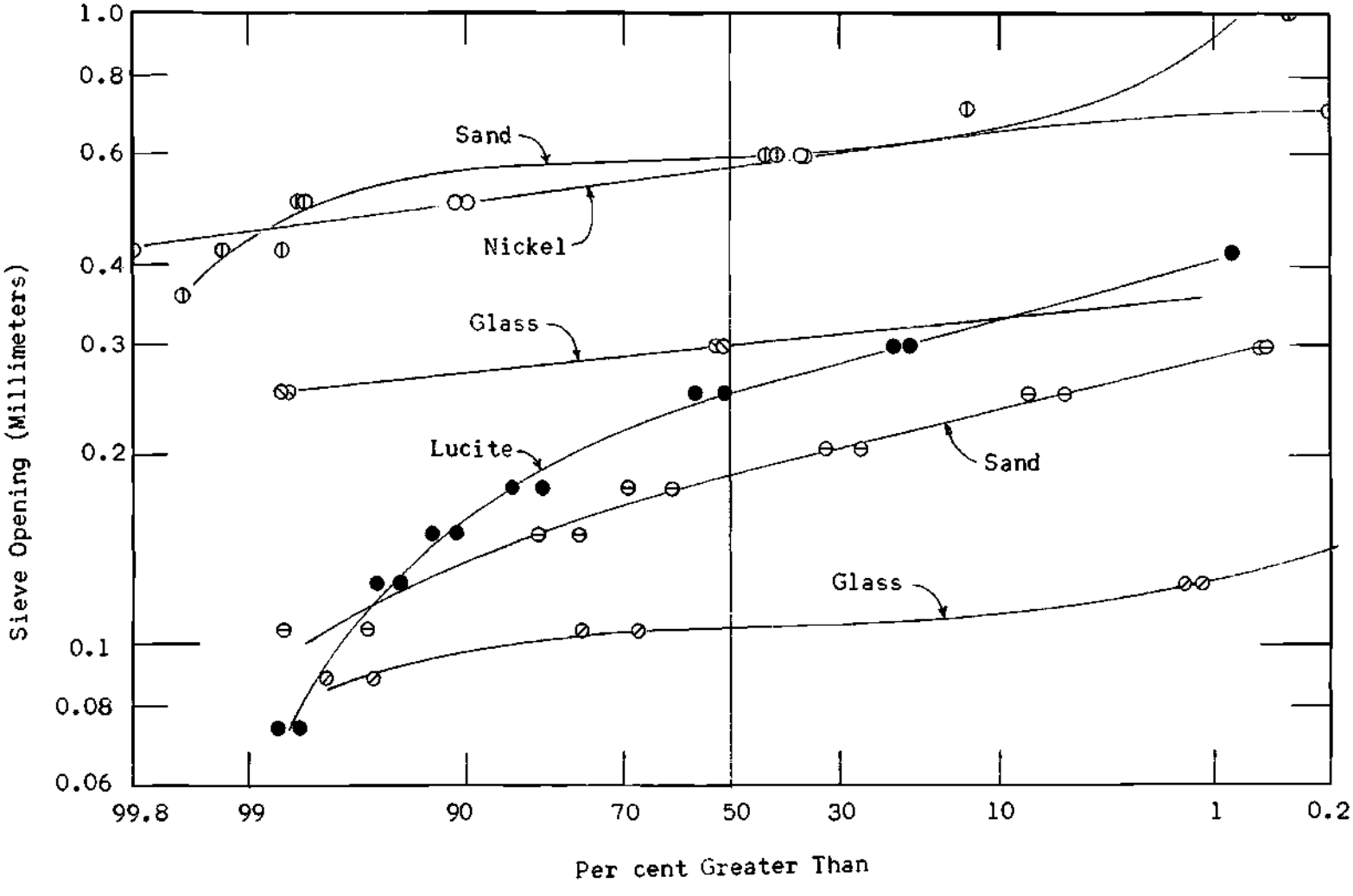

Figure 17. Sieve Analysis.

APPENDIX C

TABLES

TABLE 1. PISTON SPEEDS (INCHES/MINUTE)

PACKARD TRANSMISSION	FORD TRANSMISSION HIGH	SECOND	LOW	REVERSE
	FOR 4:13 CHAIN RATIO			
HIGH	0.3077	0.1657	0.0085	0.0820
SECOND	0.2018	0.1086	0.0643	0.0539
LOW	0.1269	0.0684	0.0405	0.0339
REVERSE	0.0968	0.0522	0.0312	0.0257
	FOR 13:4 CHAIN RATIO			
HIGH	3.250	1.751	1.040	0.867
SECOND	2.132	1.147	0.679	0.569
LOW	1.340	0.722	0.428	0.358
REVERSE	1.023	0.552	0.329	0.272

TABLE 2. SEDIMENT PROPERTIES

MATERIAL	MEAN DIAMETER MM.	SPECIFIC GRAVITY	POROSITY
NICKEL	0.570	8.75	0.501
SAND	0.585	2.62	0.499
SAND	0.185	2.63	0.512
GLASS	0.297	2.47	0.513
GLASS	0.106	2.46	0.512
LUCITE	0.250	1.20	0.517

TABLE 3. SCOUR-HOLE TEST DATA

SEDIMENT: NICKEL

DIAMETER: 0.560 MM

AVERAGE VELOCITY FEET PER SECOND	PISTON SPEED INCHES PER MINUTE
8.5500	0.0522
8.8500	0.1269
9.2500	0.3077
8.8000	0.0968
8.1000	0.0312
8.0500	0.0257
9.0800	0.2018
9.6000	0.5520
11.3500	1.3400
12.2500	3.2500
10.8000	2.1320
10.6000	1.0230
9.4500	0.3290
11.4000	2.1320
12.3000	3.2500
10.8800	1.3400
9.8800	0.5520
10.3500	1.0230

TABLE 4. SCOUR-HOLE TEST DATA

SEDIMENT: SAND

DIAMETER: 0.585 MM

AVERAGE VELOCITY FEET PER SECOND	PISTON SPEED INCHES PER MINUTE
4.5700	1.1250
4.2900	0.4640
4.0100	0.1910
3.8200	0.0940
4.6000	0.7380
4.1500	0.3540
3.9000	0.1140
4.7500	1.1250
3.8500	0.0940
4.4500	0.7380
4.1500	0.3540
5.5100	3.2500
5.4200	3.2500
4.2500	0.2720
5.2400	2.1320
4.8000	1.0230
4.4000	0.5520
5.0500	2.1320
4.3500	1.0230
3.6600	0.0257
4.2500	0.3077
3.9200	0.1269
3.6100	0.0522
3.7000	0.0312
3.5500	0.0257
3.9000	0.0948

TABLE 5. SCOUR-HOLE TEST DATA

SEDIMENT: SAND

DIAMETER: 0.185 MM

AVERAGE VELOCITY FEET PER SECOND	PISTON SPEED INCHES PER MINUTE
3.1500	0.3077
2.8000	0.1269
2.5200	0.0522
2.3200	0.0257
2.3700	0.0312
2.6700	0.0968
2.8800	0.2018
3.0700	0.3077
2.6400	0.0940
2.8500	0.1910
3.2800	0.4640
3.7200	1.1250
3.5500	0.7380
3.1300	0.3540
3.3200	0.4640
5.7500	3.2500
3.8000	1.0230
4.0500	1.3400
4.7500	2.1320

TABLE 6. SCOUR-HOLE TEST DATA

SEDIMENT: GLASS

DIAMETER: 0.297 MM

AVERAGE VELOCITY FEET PER SECOND	PISTON SPEED INCHES PER MINUTE
2.8500	0.1269
2.7000	0.0968
2.6000	0.0522
2.5000	0.0312
2.5500	0.0257
3.0800	0.3077
3.0800	0.2018
3.1200	0.3077
2.9000	0.1269
2.6700	0.0968
3.2800	0.3077
2.6500	0.0522
3.5600	0.5520
3.6800	1.3400
4.4100	3.2500
3.9000	2.1320
3.5900	1.0230
3.5900	1.0230
3.2500	0.3290
3.1200	0.2720
3.3200	0.5520
3.6500	1.3400
4.4500	3.2500
4.0500	2.1320
3.6100	1.0230
3.1700	0.3290
3.1500	0.2720
2.4700	0.0257
2.5500	0.0522
2.7900	0.1269
2.7500	0.0968
2.9000	0.2018

TABLE 7. SCOUR-HOLE TEST DATA

SEDIMENT: GLASS

DIAMETER: 0.106 MM

AVERAGE VELOCITY FEET PER SECOND	PISTON SPEED INCHES PER MINUTE
2.4600	0.0968
2.1800	0.0312
2.6500	0.2018
2.8000	0.3077
2.5600	0.1269
2.2200	0.0522
2.1200	0.0257
2.2700	0.0522
2.5000	0.1269
2.4600	0.0968
2.0600	0.0257
2.7600	0.3077
2.8000	0.3077
2.8500	0.3290
3.3800	1.0230
4.1200	2.1320
4.4900	3.2500
4.4900	3.2500
4.2700	2.1320
3.6100	1.3400
3.1500	0.5520
2.7800	0.2720
2.9000	0.3290
3.1000	0.5520
3.4700	1.0230
3.7000	1.3400
4.2000	2.1320
4.0400	3.2500
4.7500	3.2500
4.7500	3.2500

TABLE A. SCOUR-HOLE TEST DATA

SEDIMENT: LUCITE

DIAMETER: 0.250 MM

AVERAGE VELOCITY FEET PER SECOND	PISTON SPEED INCHES PER MINUTE
1.9500	1.3400
1.5500	0.2720
2.6000	3.2500
1.6700	0.5520
2.3500	2.1320
1.6200	0.3290
1.7300	1.0230
2.0500	2.1320
1.9400	1.0230
1.5800	0.3290
2.3000	3.2500
1.6900	0.5520
1.7600	1.3400
1.6000	0.3077
1.0600	0.0257
1.2100	0.0522
1.4000	0.1269
1.4500	0.2018
1.2700	0.0968
1.4000	0.1269
1.4400	0.2018
1.0500	0.0257
1.0600	0.0312

TABLE 9. PLANE-BED TEST DATA

SEDIMENT: NICKEL

DIAMETER: 0.560 MM

AVERAGE VELOCITY FEET PER SECOND	PISTON SPEED INCHES PER MINUTE
1.8400	0.3077
1.7200	0.1269
1.6200	0.0522
1.6000	0.0257
1.6200	0.0312
1.6500	0.0948
1.7000	0.2018
1.7400	0.2720
1.9200	0.5520
2.0700	1.3400
2.0600	1.0230
1.8000	0.3290

TABLE 10. PLANE-BED TEST DATA

SEDIMENT: SAND

DIAMETER: 0.585 MM

AVERAGE VELOCITY FEET PER SECOND	PISTON SPEED INCHES PER MINUTE
1.1900	0.2720
1.2400	0.5520
1.3100	1.3400
1.4000	3.2500
1.4000	3.2500
1.3600	2.1320
1.2200	1.0230
1.2000	0.3290
1.2000	0.3070
1.1500	0.1269
1.1200	0.0522
1.0700	0.0257
1.0900	0.0312
1.1400	0.0968
1.1900	0.2018

TABLE 11. PLANE-BED TEST DATA

SEDIMENT: SAND

DIAMETER: 0.185 MM

AVERAGE VELOCITY FEET PER SECOND	PISTON SPEED INCHES PER MINUTE
1.5400	0.3077
1.3800	0.1269
1.2900	0.0522
1.1800	0.0257
1.2000	0.0312
1.3400	0.0968
1.4500	0.2018
1.4500	0.2720
1.6000	0.5520
1.7500	1.3400
1.9700	3.2500
1.9700	3.2500
1.8500	2.1320
1.6900	1.0230
1.5200	0.3290

TABLE 12. PLANE-BED TEST DATA

SEDIMENT: GLASS

DIAMETER: 0.297 MM

AVERAGE VELOCITY FEET PER SECOND	PISTON SPEED INCHES PER MINUTE
1.3300	0.2720
1.4200	0.5520
1.5500	1.3400
1.7200	3.2500
1.6500	2.1320
1.5000	1.0230
1.3600	0.3290
1.3600	0.3077
1.2500	0.1269
1.1200	0.0522
1.1000	0.0257
1.1100	0.0312
1.2000	0.0968
1.3100	0.2018

TABLE 13. PLANE-BED TEST DATA

SEDIMENT: GLASS

DIAMETER: 0.106 MM

AVERAGE VELOCITY FEET PER SECOND	PISTON SPEED INCHES PER MINUTE
1.6400	0.3077
1.5000	0.1269
1.2900	0.0522
1.1800	0.0257
1.2200	0.0312
1.4400	0.0968
1.5700	0.2018
1.6100	0.2720
1.7500	0.5520
1.9200	1.3400
2.1000	3.2500
1.9200	2.1320
1.8100	1.0230
1.6200	0.3290

TABLE 14. PLANE-BED TEST DATA

SEDIMENT: LUCITE

DIAMETER: 0.250 MM

AVERAGE VELOCITY FEET PER SECOND	PISTON SPEED INCHES PER MINUTE
0.7000	0.2720
0.7400	0.5590
0.8200	1.3400
0.9700	3.2500
0.8800	2.1320
0.7800	1.0230
0.7100	0.3290
0.6900	0.3077
0.6000	0.1269
0.6000	0.0968
0.5200	0.0312
0.4900	0.0257
0.5700	0.0522
0.6600	0.2018

TABLE 15. SIEVE ANALYSIS

SEDIMENT: NICKEL

MEAN DIAMETER: 0.570 MM.

U.S. SIEVE NUMBER	SIEVE OPENING MM.	PERCENT RETAINED (BY WEIGHT) RUN NO. 1	RUN NO. 2
25	0.707	0.10	0.20
30	0.595	37.10	36.10
35	0.500	55.00	53.60
40	0.420	7.60	9.60
45	0.354	0.20	0.50
50	0.297	0.0	0.0

TABLE 16. SIEVE ANALYSIS

SEDIMENT: SAND

MEAN DIAMETER: 0.585 MM.

U.S. SIEVE NUMBER	SIEVE OPENING MM.	PERCENT RETAINED (BY WEIGHT) RUN NO. 1	RUN NO. 2
18	1.000	0.04	
20	0.841		0.16
25	0.707		12.79
30	0.595	42.67	30.89
35	0.500	56.29	54.38
40	0.420	1.33	0.25
45	0.354		1.18
50	0.297	0.57	
60	0.250	0.06	
PAN		0.04	0.35

TABLE 17. SIEVE ANALYSIS

SEDIMENT: SAND

MEAN DIAMETER: 0.185 MM.

U.S. SIEVE NUMBER	SIEVE OPENING MM.	PERCENT RETAINED (BY WEIGHT) RUN NO. 1	RUN NO. 2
50	0.297	0.55	0.50
60	0.250	7.15	5.00
70	0.210	19.20	27.00
80	0.177	34.60	36.40
100	0.149	15.40	13.50
140	0.105	19.20	16.00
PAN		3.90	1.50

TABLE 18. SIEVE ANALYSIS

SEDIMENT: GLASS

MEAN DIAMETER: 0.297 MM.

U.S. SIEVE NUMBER	SIEVE OPENING MM.	PERCENT RETAINED (BY WEIGHT) RUN NO. 1	RUN NO. 2
40	0.420	0.0	0.0
45	0.354	0.04	0.14
50	0.297	51.43	52.94
60	0.250	47.00	45.32
70	0.210	1.46	1.52
80	0.177	0.07	0.07
PAN		0.0	0.01

TABLE 19. SIEVE ANALYSIS

SEDIMENT: GLASS

MEAN DIAMETER: 0.106 MM.

U.S. SIEVE NUMBER	SIEVE OPENING MM.	PERCENT RETAINED (BY WEIGHT) RUN NO. 1	RUN NO. 2
100	0.149	0.0	0.10
120	0.125	1.50	1.10
140	0.105	66.00	75.30
170	0.088	28.40	20.90
PAN		4.10	2.50

TABLE 20. SIEVE ANALYSIS

SEDIMENT: LUCITE

MEAN DIAMETER: 0.250 MM.

U.S. SIEVE NUMBER	SIEVE OPENING MM.	PERCENT RETAINED (BY WEIGHT) RUN NO. 1	RUN NO. 2
40	0.420	0.80	0.80
50	0.297	18.80	21.20
60	0.250	31.90	35.20
80	0.177	30.50	28.40
100	0.149	8.90	7.20
120	0.125	3.70	2.90
200	0.074	3.60	2.90
PAN		1.80	1.40

TABLE 21. POROSITY TEST DATA

SEDIMENT: NICKEL

MEAN DIAMETER: 0.570 MM.

SPECIFIC GRAVITY: 8.75

SAMPLE NUMBER	PISTON DISPLACEMENT CU. CM.	DRY WEIGHT GRAMS	SEDIMENT VOLUME CU. CM.	POROSITY
1	2.817	12.23	1.40	0.503
2	2.817	11.60	1.33	0.529
3	5.634	25.13	2.87	0.491
4	2.817	12.77	1.46	0.481
				AV. 0.501

TABLE 22. POROSITY TEST DATA

SEDIMENT: SAND

MEAN DIAMETER: 0.585 MM.

SPECIFIC GRAVITY: 2.62

SAMPLE NUMBER	PISTON DISPLACEMENT CU. CM.	DRY WEIGHT GRAMS	SEDIMENT VOLUME CU. CM.	POROSITY
1	8.451	11.35	4.33	0.488
2	8.451	10.94	4.18	0.506
3	8.451	11.04	4.22	0.500
4	14.085	18.13	6.91	0.503
				AV. 0.499
	WITHOUT TAP COMPACTING			
1	8.451	9.57	3.65	0.567
2	8.451	10.77	4.11	0.514
3	8.451	10.23	3.91	0.538
4	11.268	14.38	5.49	0.513
				AV. 0.533

TABLE 23. POROSITY TEST DATA

SEDIMENT: SAND

MEAN DIAMETER: 0.185 MM.

SPECIFIC GRAVITY: 2.63

SAMPLE NUMBER	PISTON DISPLACEMENT CU. CM.	DRY WEIGHT GRAMS	SEDIMENT VOLUME CU. CM.	POROSITY
1	8.451	11.23	4.27	0.495
2	8.451	10.60	4.03	0.524
3	8.451	10.82	4.11	0.513
4	8.451	10.72	4.07	0.518
				AV. 0.512
	WITHOUT TAP COMPACTING			
1	8.451	9.91	3.77	0.553
2	8.451	9.95	3.78	0.553
3	8.451	10.22	3.89	0.540
4	14.085	16.60	6.31	0.552
				AV. 0.549

TABLE 24. POROSITY TEST DATA

SEDIMENT: GLASS

MEAN DIAMETER: 0.297 MM.

SPECIFIC GRAVITY: 2.47

SAMPLE NUMBER	PISTON DISPLACEMENT CU. CM.	DRY WEIGHT GRAMS	SEDIMENT VOLUME CU. CM.	POROSITY
1	8.451	10.43	4.23	0.500
2	8.451	10.21	4.14	0.510
3	11.268	13.50	5.46	0.516
4	14.085	16.66	6.74	0.521
5	14.085	17.21	6.96	0.506
6	16.902	19.79	8.01	0.526
				AV. 0.513

TABLE 25. POROSITY TEST DATA

SEDIMENT: GLASS

MEAN DIAMETER: 0.106 MM.

SPECIFIC GRAVITY: 2.46

SAMPLE NUMBER	PISTON DISPLACEMENT CU. CM.	DRY WEIGHT GRAMS	SEDIMENT VOLUME CU. CM.	POROSITY
1	8.451	10.58	4.30	0.491
2	8.451	10.14	4.12	0.513
3	8.451	9.91	4.03	0.523
4	11.268	13.24	5.38	0.523
				AV. 0.512
	WITHOUT TAP COMPACTING			
1	8.451	9.59	3.90	0.538
2	8.451	9.60	3.90	0.538
3	8.451	9.59	3.90	0.538
				AV. 0.538

TABLE 24. POROSITY TEST DATA

SEDIMENT: LUCITE

MEAN DIAMETER: 0.250 MM.

SPECIFIC GRAVITY: 1.20

SAMPLE NUMBER	PISTON DISPLACEMENT CU. CM.	DRY WEIGHT GRAMS	SEDIMENT VOLUME CU. CM.	POROSITY
	11.268	6.82	5.68	0.496
	11.268	6.25	5.21	0.538
	8.451	4.95	4.12	0.512
	11.268	6.51	5.42	0.520
	8.451	4.91	4.09	0.516
	11.268	6.48	5.40	0.521
	14.085	8.24	6.86	0.514
	14.085	8.13	6.77	0.520
				AV. 0.517

TABLE 27. VELOCITY PROFILE

AVERAGE VELOCITY=57.7 FT./SEC.
BAROMETER=29.77 IN. HG.
AIR TEMPERATURE=71 DEGREES F.
CATHOMETER ZERO=471.95 MM.
MANOMETER ZERO=5.513 IN. WATER

CATHOMETER READING MM.	MANOMETER READING INCHES	DISTANCE FROM BOUNDARY FEET	VELOCITY FT./SEC.
472.15	5.5360	0.0007	10.2144
472.40	5.6800	0.0015	27.5237
472.75	5.9300	0.0026	43.4927
472.90	6.0060	0.0031	47.2903
473.25	6.1350	0.0043	53.1183
473.45	6.1820	0.0049	55.0886
473.70	6.2130	0.0057	56.3505
474.05	6.2380	0.0069	57.3479
474.45	6.2570	0.0082	58.0945
475.00	6.2700	0.0100	58.5999
475.80	6.2780	0.0126	58.9087
476.60	6.2840	0.0153	59.1392
478.60	6.2840	0.0218	59.1392
480.75	6.2840	0.0289	59.1392
483.70	6.2960	0.0386	59.5977
486.10	6.3040	0.0464	59.9014
488.60	6.3040	0.0546	59.9014
491.30	6.3040	0.0635	59.9014
497.70	6.3200	0.0845	60.5042
502.55	6.3200	0.1004	60.5042
509.00	6.3200	0.1216	60.5042

TABLE 28. VELOCITY PROFILE

AVERAGE VELOCITY=26.2 FT./SEC.
BAROMETER=29.26 IN. HG.
AIR TEMPERATURE=74 DEGREES F.
CATHOMETER ZERO=472.00 MM.
MANOMETER ZERO=5.523 IN. WATER

CATHOMETER READING MM.	MANOMETER READING INCHES	DISTANCE FROM BOUNDARY FEET	VELOCITY FT./SEC.
472.00	5.5230	0.0000	0.0000
472.25	5.5280	0.0008	4.8147
472.50	5.5360	0.0016	7.7636
472.90	5.5800	0.0030	16.2565
473.25	5.6150	0.0041	20.6530
473.55	5.6400	0.0051	23.2907
473.75	5.6520	0.0057	24.4559
474.00	5.6600	0.0066	25.2028
474.50	5.6680	0.0082	25.9282
475.20	5.6740	0.0105	26.4592
476.25	5.6800	0.0139	26.9798
478.30	5.6830	0.0207	27.2363
481.70	5.6840	0.0318	27.3213
488.70	5.6870	0.0548	27.5747
496.40	5.6890	0.0801	27.7423
506.10	5.6910	0.1119	27.9089
513.70	5.6910	0.1368	27.9089

TABLE 29. RANGE OF d/δ^*

MATERIAL	DIAMETER MM.	MINIMUM	MAXIMUM
NICKEL	0.570	0.665	0.756
SAND	0.585	0.558	0.638
SAND	0.185	0.185	0.239
GLASS	0.297	0.287	0.359
GLASS	0.106	0.106	0.142
LUCITE	0.250	0.161	0.227

TABLE 30. INCIPIENT-MOTION DATA

MATERIAL	DIAMETER MM.	CRITICAL AVERAGE VELOCITY (FEET/SECOND) PLANE BED	SCOUR HOLE
NICKEL	0.570	1.30	7.00
SAND	0.585	0.63	2.75
SAND	0.185	0.70	1.45
GLASS	0.297	0.60	1.83
GLASS	0.106	0.63	1.23
LUCITE	0.250	0.29	0.64

REFERENCES

1. Brown, C. B. "Sediment Transportation," Engineering Hydraulics, H. Rouse ed., John Wiley and Sons, New York, 1950, p. 795.

2. DuBoys, P., "Le Rhone et les rivieres a lit affouillable," Annales des ponts et chaussees, series 5, Vol. 18, 1879, pp. 141-195 as referenced in Engineering Hydraulics, H. Rouse ed.

3. Shields, A., "Anwendung der Aehnlichkeitsmechanik und der Turbulenzforschung auf die Geschiebebewegung," Mitteitungen der Preusschen Versuchanstalt für Wasserbau and Schiffbau, Berlin, Vol. 26, 1936. (Translation in Engineering Societies Library, New York).

4. Garde, R. J., "Total Sediment Transport in Alluvial Channels," Doctoral Dissertation, Colorado State University, Fort Collins, Colorado, January 1959.

5. Brooks, N. H., "Mechanics of Streams with Movable Beds of Fine Sand," Transactions, American Society of Civil Engineers, Vol. 123, 1958, pp. 526-549.

6. Rouse, H., "Criteria for Similarity in the Transportation of Sediment," Proceedings Hydraulics Conference, University of Iowa Studies in Engineering, Bulletin 20, 1940, pp. 33-49.

7. Laursen, E. M., "Observations on the Nature of Scour," Proceedings 5th Hydraulics Conference, State University of Iowa, Bulletin 34, 1952, pp. 179-197.

8. Laursen, E. M. and Toch, A., "A Generalized Model Study of Scour Around Bridge Piers and Abutments," Proceedings, Minnesota International Hydraulics Convention, Minneapolis, Minn., 1953, pp. 123-131.

9. Ahmed, M., "Experiments on Design and Behavior of Spur Dikes," Proceedings, Minnesota International Hydraulics Convention, Minneapolis, Minn., 1953, pp. 145-159.

10. Carstens, M. R., Unpublished study, School of Civil Engineering, Georgia Institute of Technology, Atlanta, Georgia.

11. Chepil, W. S., "The Use of Evenly Spaced Hemispheres to Evaluate Aerodynamic Forces on a Soil Surfaces," Transactions, American Geophysical Union, Vol. 39, No. 3, June 1958, pp. 397-404.

12. Young, D. F., "Drag and Lift on Spheres Within Cylindrical Tubes," Transactions, American Society of Civil Engineers, Vol. 126, Part I, 1961, pp. 1235-1245.

13. Rouse, H., Engineering Hydraulics, John Wiley and Sons, New York, 1950, p. 122.

14. Ibid, p. 103.

15. Nikuradse, J., "Laws of Flow in Rough Pipes," translated as Tech. Memo 1292, National Advisory Committee for Aeronautics, Washington, D. C., 1950.

16. Schlichting, H., Boundary Layer Theory, McGraw-Hill, 4th Ed., New York, 1960, p. 116.

17. Blasius, H., "Grenzschichten in Flussigkeiten mit kleiner Reibund Z. Math u Phys. 56, 1 (1908). English translation in NACA Tech. Memo. No. 1256.

18. Schlichting, H., Boundary Layer Theory, McGraw-Hill, 4th Ed., New York, 1960, p. 123.

19. Ibid., p. 122

20. Ibid., p. 379.

21. Feindt, E. G., "Unter suchungen über die Akhängigkeit des Umschlages laminar-turbulent von der Oberflächenrauhigkeit und der Druckverteilung," Thesis Braunschweig 1956; as referenced in Schlichting (18), p. 449.

VITA

Albert Richard LeFeuvre was born in Toronto, Ontario, Canada, on March 15, 1928. He attended local schools and graduated from Northern Vocational School, Toronto, Canada in 1946. In 1949, he completed the university entrance requirements and graduated from the University of Toronto with a Bachelor of Applied Science in Mechanical Engineering in June of 1953. He was employed by the Dominion Oxygen Company of Toronto, Canada from June of 1953 to September of 1954. At that time he resumed his education at the University of Toronto where he was employed as a Laboratory Demonstrator while working towards his Masters Degree. During the summers of 1955, 1956, and 1957 he was employed by the Hydro-Electric Power Commission of Ontario, Hydraulic Models Laboratory, Islington, Ontario. He graduated from the University of Toronto with a Master of Applied Science in Mechanical Engineering in June of 1956. During the academic year 1956-1957 he was employed by the University of Toronto as an Instructor of Mechanical Engineering. In January of 1958 he joined the faculty of the University of Waterloo, Waterloo, Ontario, Canada. He presently holds the rank of Assistant Professor of Mechanical Engineering at the University of Waterloo.

In September of 1962 he took a leave of absence to attend the Georgia Institute of Technology in pursuit of a Doctor of Philosophy degree. While at this school, he was employed as a graduate teaching assistant. He was a recipient of a Ford Foundation Fellowship-Assistantship for prospective engineering teachers during the period from September

1963 to June 1965.

He is an associate member of the honorary society, Sigma Xi. He is also a member of the following professional societies: American Society for Engineering Education, American Society of Civil Engineers, and the Ontario Association of Professional Engineers.

He is married and has two sons.